Hindawi
Shock and Vibration
Volume 2023, Article ID 8822754, 24 pages
https://doi.org/10.1155/2023/8822754

Research Article

Response Characteristics and Suppression of Transverse Vibrations of Mine Hoisting Conveyances Excited by Multiple Faults

Jiannan Yao, Di Liu, and Xiaojie Deng

School of Mechanical Engineering, Nantong University, Nantong 226019, China

Correspondence should be addressed to Jiannan Yao; yaojiannan1988@163.com

Received 1 June 2023; Revised 22 August 2023; Accepted 4 September 2023; Published 15 September 2023

Academic Editor: Biao Xiang

The failures of steel guides can excite complex and intense transverse oscillations of hoisting containers in the mine hoisting process. The present paper mainly contributes to reveal the response characteristics of the transverse oscillations of mine conveyances excited by various faults such as interface misalignment, local bulge, orbital gap, bending deformation, and orbital tilt. First, a rigid-flexible coupled virtual prototype model between the conveyance and the steel guide was established. Subsequently, the vibration response characteristics of the container under various single and coupling excitations were simulated and analyzed. Eventually, a new type of roller cage shoe with a magnetorheological damper was put forward to decrease the transverse impact responses. Based on the hyperbolic tangent model of magnetorheological dampers, a semiactive fuzzy PID method was studied to explore the vibration suppression of the container. The results showed the fuzzy PID method can play a good role in the vibration reduction. This paper can give a fine scheme for the virtual simulation and semiactive vibration control of the mine hoisting system.

1. Introduction

As shown in Figure 1, rigid guides are usually employed to keep the containers moving up and down in the vertical shaft [1]. However, in the practical operation processes, due to guide faults such as interface misalignment, local bulge, orbital gap, bending deformation, and orbital tilt [2], as shown in Figure 2, abnormal transverse vibrations of the hoisting conveyance may be excited and then deteriorate the hoisting stability of the system, sometimes causing serious accidents such as the conveyance blocking. Hence, it is significant to investigate the corresponding oscillation characteristics under the conditions of the various guide faults and propose a reasonable suppression scheme.

Some scholars have completed a lot of meaningful work concerning mine hoist dynamics. Yao et al. [1, 3] have investigated the longitudinal impact responses of the mine hoisting system excited by interface misalignment, but they have not mentioned the corresponding transverse response characteristics. Ma et al. [2] have built the models of rigid guides with different sorts of defects on a test rig and collected the signals of vibration and angle to perform pattern recognition of rigid guides. Wang et al. [4] have used Hamilton's principle to establish the nonlinear hoisting dynamic model and then investigated the longitudinal vibration responses. Zhu et al. [5] have established a virtual prototype model of the catenary of a mine hoist in Adams and proposed a new device to suppress the catenary transverse oscillations. Guo et al. [6, 7] have explored the tensile and vibration characteristics of the longitudinal vibrations of the friction-drive hoist experimentally. Wang et al. [8] have deduced the dynamic equations of the mine hosting system using Hamilton's principle, and then the model was verified by comparing it to the virtual simulation results. Ma et al. [9] have simulated the cage vibration responses under different fault excitations and cage operating conditions. Cao et al. [10] have investigated the transient responses of the mine hoist subjected to driving deviations.

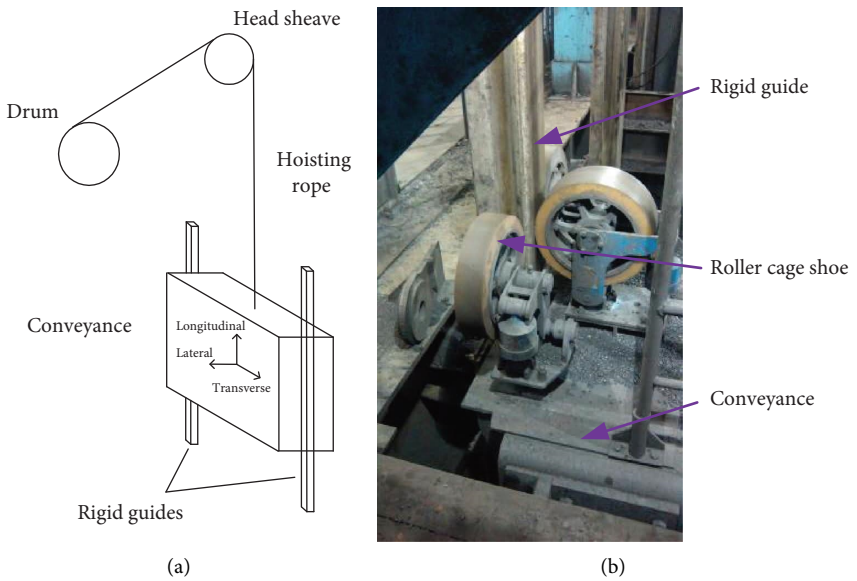

Figure 1: Schematic diagram of the structure for a mine hoist: (a) equipment form; (b) practical situation.

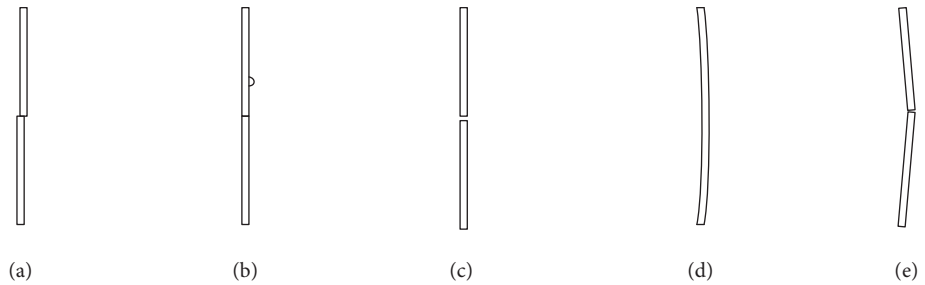

Figure 2: Various defects of rigid guide: (a) interface misalignment, (b) local bulge, (c) orbital gap, (d) bending deformation, and (e) orbital tilt.

In elevator systems similar to mine hoisting systems, Yang et al. [11] have established a dynamical model of elevator transverse vibration based on Lagrange's principle. Fluid dynamics was considered to study the transverse vibration characteristics. Peng et al. [12] have analyzed the vibration responses when the machine was under emergency braking. Zhang et al. [13, 14] have analyzed the effects of random parameters and excitations on the nonlinear vibration characteristics of the rolling guide shoe. Yang et al. [15] derived an elevator dynamic model, and the accuracy of the model was verified experimentally. Zhou et al. [16] have analyzed the influences of the disturbance frequency and the operating speed on the horizontal vibrations of the elevator system. Zhang et al. [17] have investigated the horizontal vibration dynamics of an elevator car under the influence of the airflow. Qiu et al. [18] have proposed an energy-based vibration model to investigate the coupling vibration characteristics of an elevator, and it was concluded that its accuracy is better than that of the conventional differential equation-based vibration model.

Research on vibration control of hoisting systems has focused on elevator systems. Benosman [19] has used displacement regulation of the elevator compensation wheel to drive the system and proposed a nonlinear controller based on Lyapunov theory to suppress vibration of the elevator ropes. Nguyen et al. [20, 21] analyzed the vibration of elevator ropes by numerically solving nonlinear equations and proposed the installation of an active controller on the compensating sheave of the elevator. The genetic algorithms were used to control the rope vibration under different seismic conditions. Santo et al. [22] have put forward a control strategy to suppress the horizontal vibration of a vertical transport elevator car by applying the state-dependent Riccati equation method. Raúl et al. [23] have proposed magnetorheological damping of semiactive guide shoes and designed the corresponding control strategy. Zhang et al. [24] have constructed an elevator system dynamics model and proposed a semiactive control method to reduce the horizontal vibration of the elevator car by employing magnetorheological damping guide shoes. Hu et al. [25] have established a quarter vehicle model and proposed a new HFFPID controller to realize the semiactive vibration control.

The semiactive fuzzy PID control method is an important method that has been used in many control systems. Zeng et al. [26] have designed a fuzzy PID controller to

control the liquid lava reactor core power by linearizing the nonlinear model using the small perturbation linearization method, and the research results demonstrated that the proposed fuzzy PID method has a better performance than the traditional PID controller. Wu et al. [27] applied vector control combined with a fuzzy PID controller to realize the dynamic control of the electromagnetic torque in a mine hoist. Ma et al. [28] have designed a mine hoist constant deceleration compensation device by using a fuzzy neural network PID control strategy. Simulink simulation and field experiments were carried out to verify the feasibility of the device. Xiao et al. [29] have established the mathematical model of a mine hoist controllable antislip device and designed the parallel-type fuzzy PID controller. Wang et al. [30] have established a simulation platform for the disk braking system of a mine hoist, designed a fuzzy PID controller for the constant deceleration emergency braking system, and carried out tests on the hoist test bench, which showed that the fuzzy PID controller can effectively control the deceleration braking. Wang et al. [31] have designed a new type of voltage regulator transformer and used the fuzzy PID control strategy to control the fluctuation of voltage amplitude in the mine power supply system.

After analyzing the literature mentioned above, further study such as the virtual simulation for revealing the transverse oscillation characteristics of the conveyance by considering the flexible coupling with the hoisting rope can be conducted, and a feasible method should be put forward to control the transverse vibrations of the conveyance in the abnormal operation environments. As a consequence, the main research focus of this paper would be different from the previous mathematical modeling simulation, using a virtual prototype simulation environment, considering the rigid-flexible coupling properties to simulate the vibration responses of the container under various typical faults. Meanwhile, a new structure of roller cage shoe was proposed, and the control algorithm was applied to the vibration suppression of the hoisting conveyance in the mine.

The article was organized as follows: (1) Section 2 describes virtual simulation models; (2) Section 3 describes transverse vibration characteristics influenced by various guide faults; (3) Section 4 describes vibration suppression by a new guide roller equipped with a magnetorheological (MR) damper; and (4) Section 5 provides conclusions.

2. Virtual Simulation Models

A virtual simulation model to describe the transverse vibration of the conveyance was established, as shown in Figure 3. The ropes are connected to both the conveyance and the drum. The conveyance is lifted up and down by means of drum winding and moves vertically on the rigid guides through the roller cage shoes, as shown in Figure 1. In the present paper, the main solution is to establish a virtual prototype model and simulation. As a multifunctional multibody dynamics simulation software, Adams has been widely used in engineering practice.

For the purpose of modeling and solving, the following model simplifications have been performed. First,

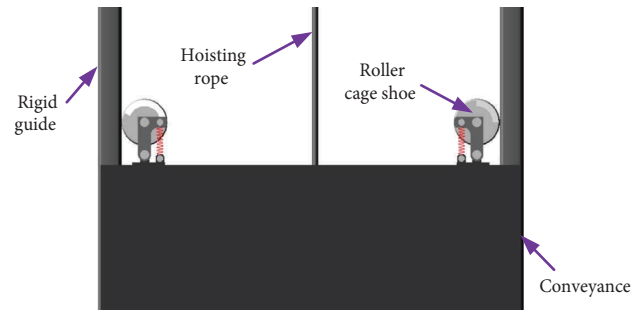

Figure 3: Modeling of transverse vibration of conveyance.

considering the complex contact force relationship between the drum and rope during the winding motion, the corresponding force calculation will result in convergence difficulties in the solution, which will reduce the efficiency of the simulation. In addition, this study aims at exploring the disturbance properties of the transverse vibrations of the hoisting conveyance by using the Adams virtual prototype environment. The influence of the movement of the rope on the drum on the conveyance is far less than that of the rigid guides, so there is no need to establish a complex drum model. Second, considering that the head sheave acts a role as a guide device, it is difficult to solve the contact force. Therefore, a moving pair can be adopted to represent the connection relationship between the rope and head sheave. Subsequently, the roller cage shoes in the horizontal direction were only considered, and the disc spring structure in the buffer was simplified as a linear spring. Based on the above engineering simplification, the present paper mainly focuses on establishing the multibody dynamics model between the conveyance, rope, roller cage shoe, and rigid guide by using the Adams virtual simulation environment to investigate the response characteristics of the transverse vibrations of the hoisting conveyance excited by multiple faults.

2.1. Coupling Model between the Conveyance and Rigid Guide. The hoisting conveyance is usually lifted up and down in the mine shaft. During the hoisting process, intense vibrations of the conveyance are usually excited by the coupling impact from the rigid guide and the roller cage shoe due to the failures such as the interface misalignment, local bulge, orbital gap, bending deformation, and orbital tilt of the rigid guide, as shown in Figure 2. Hence, it is necessary to establish the coupling model between the conveyance and rigid guide to reveal the effects of the various faults on the transverse vibrations of the container.

The conveyance and rigid guide are simple in construction. The conveyance can be approximated as a cuboid, and the rigid guide is a square steel pipe with a certain wall thickness. The roller cage shoe is a key component to maintain the hoisting stability for the conveyance along the rigid guide. The roller cage shoe consists of a polyurethane roller, rocker arm, buffer, and base, as shown in Figure 4. During the conveyance motion process, when the polyurethane rollers which are rigidly installed on the

conveyance are pressed on the rigid guide, the rocker arm will be pressed on the buffer that consists of multiple disc springs to reduce the impact influence to a certain extent. In the present paper, a type of roller cage shoe with a roller diameter of 0.35 m was selected as the research object for the following modeling and simulation.

To establish the virtual prototype model of the selected roller cage shoe, the three-dimensional model was first built in SolidWorks and then imported into Adams in the format of Parasolid ($*.X\_T$). To realize the virtual simulation, the material properties and constraint relationships of all parts should be set in the software.

The outer ring material of the roller is polyurethane [9], which has a density, modulus of elasticity, and Poisson's ratio of $1.0\times10^3\,\mathrm{kg/m^3}$, $2.5\times10^7\,\mathrm{N/m^2}$, and 0.49. The material of the rest of the parts was set to steel, and its density, modulus of elasticity, and Poisson's ratio are $7.8\times10^3\,\mathrm{kg/m^3}$, $2.07\times10^{11}\,\mathrm{N/m^2}$, and 0.29.

A fixed pair was first set between the conveyance and the base of the roller cage shoe which is rigidly fixed on the conveyance. The linear spring, simplified by buffer, was set between the rocker arm and base. Subsequently, the restraint relationships among the base, rocker arm, polyurethane roller, and bolts were set, as shown in Table 1.

The coupled constraint between the polyurethane roller and the rigid guide mainly exists in the form of a contact force. In the Adams simulation environment, the formula for contact force during a collision is usually expressed by the following impact function [32]:

$$F=\begin{cases}0, & q>q_0,\\ k\left(q_0-q\right)^e-C_{\max}\cdot\left(\dfrac{dp}{dt}\right)\cdot\operatorname{step}\left(q,q_0-d,1,q_0,0\right), & q\le q_0,\end{cases}\tag{1}$$

where q_0 is the initial distance between the two objects to collide, $q_0=0$; q is the actual distance between two objects during collision; k is the stiffness; e is the force exponent which is generally 2; $c_{\max}$ is the maximum damping coefficient which is usually 0.1%~1% to the value of the stiffness coefficient; dq/qt is the rate at which the distance between two objects changes with time; and d is the penetration depth, it determines when the damping force reaches its maximum value. When the collision occurs, there is no damping force. As the penetration depth increases, the damping force increases until it reaches its maximum value. Its suitable value is 0.1 mm. The stiffness coefficient of a collision of a rotating object can be approximately determined according to the following equation: $k=4/3{*}R^{1/2}{*}E$. In the formula: $1/R=1/R_1+1/R_2$, R_1 and R_2 are the radius of the collision point of the two collisions; $1/E=(1-\nu_1^2)/E_1+(1-\nu_2^2)/E_2$; ν_1 and ν_2 are Poisson's ratios of two objects, respectively; E_1 and E_2 are elastic moduli of two objects, respectively. Since the two impacting objects are a polyurethane roller and a rigid guide. Their radius and material are known and can be obtained at $k=1.835\times10^7\,\mathrm{N/m}$. To prevent discontinuities in the damping force during a collision, the step function is used in the form of steps (x, x_0, h_0, x_1, and h_1):

$$\operatorname{step}=\begin{cases}h_0, & x\le x_0,\\ h_0+a\cdot\Delta^2\left(3-2\Delta\right), & x_0<x<x_1,\\ h_1, & x\ge x_1.\end{cases}\tag{2}$$

In the following equation:

$$a=h_1-h_0;\Delta=\frac{\left(x-x_0\right)}{\left(x_1-x_0\right)}.\tag{3}$$

When the roller cage shoe collides with the rigid guide due to the various faults of the guide such as the interface misalignment, local bulge, orbital gap, bending deformation, and orbital tilt, as shown in Figure 2, the actual distance between the two objects will vary in terms of the disturbance extent from the abovementioned guide failures. Various fault settings for rigid guides would be highlighted in the simulation section.

2.2. Modeling of Rope. The hoisting wire rope is used to connect to the conveyance and it ensures that the conveyance could be lifted up and down in the mine shaft. The increase in the depth of the mine shaft directly results in a large increase in the length of the wire rope, which in turn enhances the flexibility of the rope body. Therefore, it is essential to come up with a suitable method to model the wire rope in order to describe its flexible characteristics. For the modeling of the rope, the method of a multisection rigid cylinder was adopted to simulate the rope [8]. This method can establish the wire rope quickly, accurately, and truly to obtain the motion characteristics of the rope. The key to this method is to treat the flexible wire rope as a series of discrete rigid cylinders connected by bushing forces. According to actual operating conditions, the length and diameter of the hoisting rope are 200 m and 76 mm, respectively [5]. If the length of each discrete cylinder is 200 mm, a total number of 1000 is required. A section of a cylinder in Adams should first be established, and then the established section should be copied and moved by using the Adams macro command program, then a bushing force would be added between every two cylinders in order to build a virtual prototype model of wire rope. The bushing force is equivalent to a spring structure with six components. By defining three

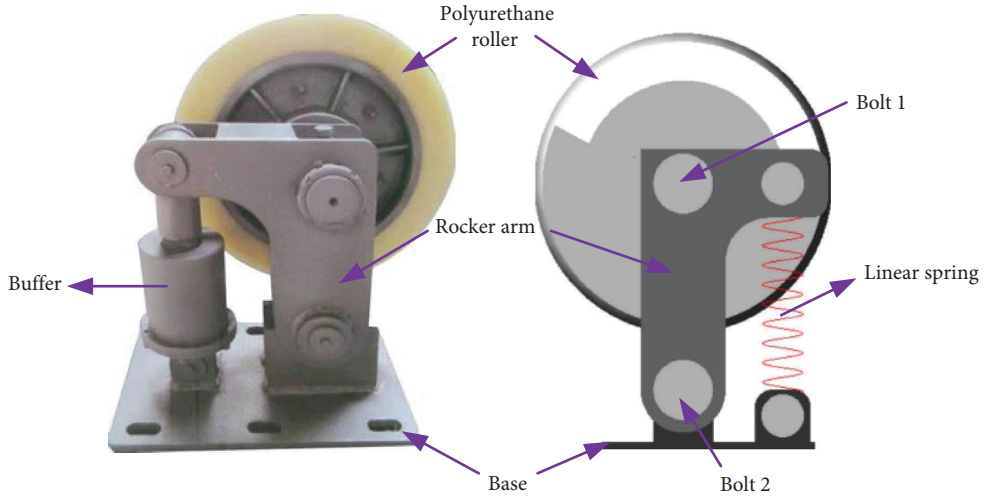

Figure 4: Roller cage shoe.

Table 1: Internal constraints of the roller cage shoe.

Part 1	Part 2	Constraint relation
Bolt 1	Polyurethane roller	Revolute pair
Bolt 1	Rocker arm	Fixed pair
Bolt 2	Rocker arm	Revolute pair
Bolt 2	Base	Fixed pair

force components $\{F_x, F_y, \text{and } F_z\}$ and three-moment components $\{T_x, T_y, \text{and } T_z\}$, a flexible force was added between the two discrete cylinders to connect the discrete model, as shown in Figure 5.

The bushing force can be calculated by the following formula:

$$\begin{bmatrix} F_x \\ F_y \\ F_z \\ T_x \\ T_y \\ T_z \end{bmatrix} = \begin{bmatrix} K_{11} & 0 & 0 & 0 & 0 & 0 \\ 0 & K_{22} & 0 & 0 & 0 & 0 \\ 0 & 0 & K_{33} & 0 & 0 & 0 \\ 0 & 0 & 0 & K_{44} & 0 & 0 \\ 0 & 0 & 0 & 0 & K_{55} & 0 \\ 0 & 0 & 0 & 0 & 0 & K_{66} \end{bmatrix} \begin{bmatrix} r_x \\ r_y \\ r_z \\ \theta_x \\ \theta_y \\ \theta_z \end{bmatrix} - \begin{bmatrix} C_{11} & 0 & 0 & 0 & 0 & 0 \\ 0 & C_{22} & 0 & 0 & 0 & 0 \\ 0 & 0 & C_{33} & 0 & 0 & 0 \\ 0 & 0 & 0 & C_{44} & 0 & 0 \\ 0 & 0 & 0 & 0 & C_{55} & 0 \\ 0 & 0 & 0 & 0 & 0 & C_{66} \end{bmatrix} \begin{bmatrix} v_x \\ v_y \\ v_z \\ \omega_x \\ \omega_y \\ \omega_z \end{bmatrix} + \begin{bmatrix} F_{x^0} \\ F_{y^0} \\ F_{z^0} \\ T_{x^0} \\ T_{y^0} \\ T_{z^0} \end{bmatrix}, \tag{4}$$

where $K_{11} \sim K_{66}$ and $C_{11} \sim C_{66}$ represent the stiffness and damping of the springs, respectively; r, θ, v, and ω denote the relative displacement, angle of rotation, velocity, and angular velocity of two neighboring cylinders, respectively. x_0, y_0, and z_0 represent the initial values in each coordinate direction. The stiffness coefficient [11] was calculated as shown in Table 2. The damping is usually between 1 and 10 Ns/mm; 5 Ns/mm was employed in the present paper.

In Table 2, E is the elastic modulus of the rope. The material of the wire rope is steel 45, and its elastic modulus is 200 GPa. A is the cross-sectional area of the wire rope; l is the length of a discrete cylinder of 200 mm; G is the shear modulus of the wire rope, $G = E/2\ (1+\mu) = 80$ GPa; μ is Poisson's ratio of 0.25; and D is the diameter of a discrete cylinder of 76 mm. According to the above steps and parameters, a virtual prototype model of wire rope can be constructed, as shown in Figure 6.

3. Research Studies on Transverse Vibrations with Single Fault and Multiple Faults

To investigate the impact response characteristics of the conveyances excited by the various faults of rigid guides using the method of virtual prototype techniques. Five operating modes of rigid guides were set, respectively, according to the five different failure modes, and the simulations under the different conditions were separately

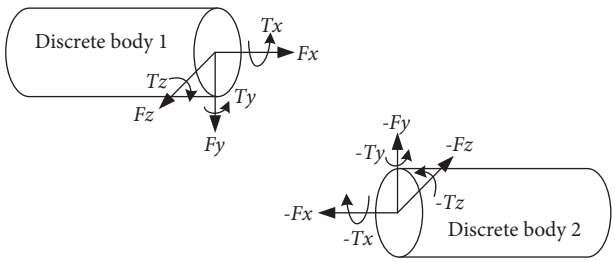

Figure 5: Schematic diagram of bushing force.

Table 2: Formulas and results of different stiffness.

Items	Formula	Results
Tensile stiffness	$K_{11} = EA/l$	1.96×10^9 N/m
Shear stiffness	$K_{22} = K_{33} = GA/l$	7.85×10^8 N/m
Torsional stiffness	$K_{44} = G\pi D^4/32l$	2.45×10^{11} Nm/rad
Bending stiffness	$K_{55} = K_{66} = E\pi D^4/64l$	3.07×10^{11} Nm

carried out. For the convenience of research, it was assumed that the guide failures exist in the steel guides which are at one side of the conveyance, and the conveyance was assumed to pass over the failure location at a constant speed. The main parameters of a hoisting system for dynamic simulation were determined, as shown in Table 3 [15]. So, to intuitively compare the influences of various faults on the transverse vibration of the container, the vibration response of the conveyance under the normal working condition of the guideway was also simulated, and the response curves are shown in Figure 7.

3.1. Responses from Interface Misalignment. Due to the installation errors or deterioration of operating conditions of the rigid guide, the height difference between the two adjacent guides will result in interface misalignment at the joint, which will cause a step excitation when the guide roller is passing over the step. The interface misalignment can be divided into two forms, as shown in Figure 8. Assuming that the step was on the steel guides which are at the one side of the conveyance, and that its height (h) is, respectively, 0.01 m, 0.02 m, 0.03 m, 0.04 m, and 0.05 m, the responses of the transverse vibration acceleration and displacement of the conveyance were simulated under the conditions of the two failure forms of the interface misalignment, as shown in Figure 8, and the response results are shown in Figure 9.

As seen from the four subfigures in Figure 9, the responses of the transverse vibration of the conveyance excited by the interface misalignment in the form, as shown in Figure 8(a), are more intense than those excited by the failure form, as shown in Figure 8(b).

It can be seen from Figures 9(a) and 9(b), when the upper guide roller which is installed on the top of the conveyance was just rolling up to the step, the transverse acceleration and displacement of the conveyance abruptly increased to the peak values. After a short time, another transverse impact acceleration and displacement were excited to peak values, respectively, when the lower guider roller which is installed on the bottom of the conveyance was just rolling up to the step. At the same time, as the height of the step increased, the amplitude of the vibration response uniformly increased, while the frequency remained basically unchanged. After the upper guide roller had already rolled up to the step, the roller was extruded and the conveyance would tilt at the same time, and continuous oscillations of the acceleration and displacement would last for about 0.6 seconds. After the lower roller had rolled up to the step, a continuous oscillation of the acceleration would last for about 6 seconds, but the transverse displacement could not be restored to 0 because the space between the two steel guides which are located at the two symmetrical edges of the conveyance became narrower.

As shown in Figures 9(c) and 9(d), for acceleration, as the height of the step increased, the amplitude and frequency of the vibration gradually decreased. When the height reached 50 mm, the amplitude after the roller passing through the step is even smaller than normal. This is because the distance between the two steel guides became very wide, making the pressure of the guideways on the roller very small. Due to the same reason, for displacement, as the height increased, the amplitude increased while the frequency decreased. When the height reached 50 mm, there was basically no vibration in the displacement.

3.2. Responses from the Local Bulge. Local bulges such as rust spots may appear on the surface of the guideway during the long-time service life of the rigid guide. Assuming that the bulge was on the steel guides which are at one side of the conveyance, and that its height is 0.01 m, 0.02 m, 0.03 m, 0.04 m, and 0.05 m. Therefore, a regular raised rust spot was drawn on a section of rigid guide surface in Adams to realize the setting of the local bulge fault, as shown in Figure 10. The height from the highest point of the bulge to the surface of the guideway was h. When the conveyance was hoisted up under this condition, the transverse acceleration and displacement of the conveyance were simulated and demonstrated, as shown in Figure 11.

As seen from Figures 11(a) and 11(b), the transverse impact acceleration and displacement of the conveyance would be excited when the upper and lower guide rollers were just passing over the bulge. For acceleration, the amplitude was very small after passing through the bulge. The amplitude and frequency remained essentially constant as h increased. The amplitude of displacement increased with an increase in h, and its frequency remained more or less constant. The vibration of displacement was very small as compared to the case of step.

3.3. Responses from Orbital Gap. A gap between the two adjacent rigid guides would be induced due to the loosening of the guideway joints. Assuming that the gap was on the steel guides which are at the one side of the conveyance, and that its width b was 0.01 m, 0.02 m, 0.03 m, 0.04 m, and 0.05 m. A rigid guide was moved up by 0.01 m, 0.02 m, 0.03 m, 0.04 m, and 0.05 m separately to create a gap to realize the orbital gap fault setting, as shown in Figure 12.

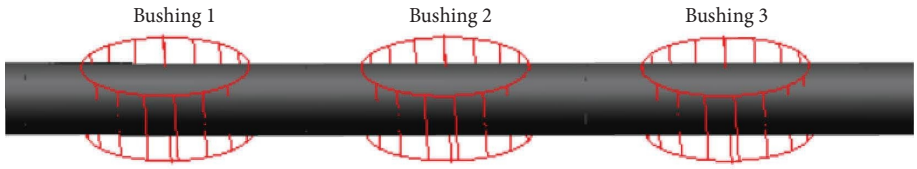

Figure 6: Schematic diagram of part of the wire rope.

Table 3: Transverse vibration simulation parameters of a hoisting conveyance.

Parameters	Numerical values	Units
Conveyance mass	3.4×10^4	kg
The moment of inertia of the conveyance with respect to the transverse direction	2.08×10^5	Kg/m^2
The moment of inertia of the conveyance with respect to the longitudinal direction	3.31×10^4	Kg/m^2
The moment of inertia of the conveyance with respect to the lateral direction	2.34×10^5	Kg/m^2
Spring stiffness	2.25×10^6	N/m
Roller diameter	0.35	m
Rope length	200	m
Rope diameter	0.076	m
Lifting time	20	s
Lifting speed	15	m/s

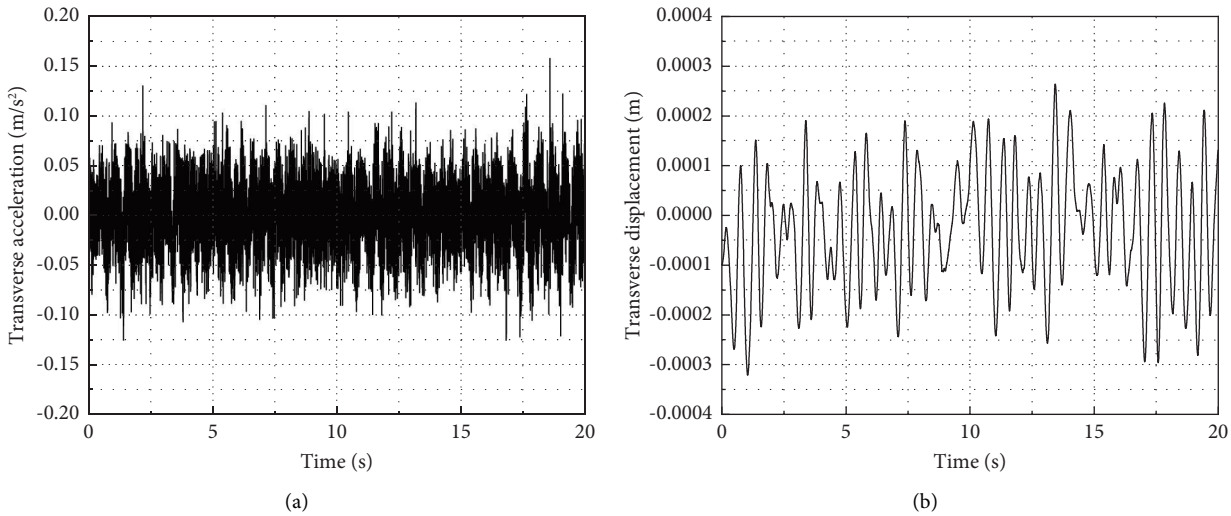

Figure 7: Transverse vibration response of under normal condition: (a) transverse acceleration; (b) transverse displacement.

When the conveyance was being hoisted up under this condition, the transverse acceleration of the conveyance was simulated and demonstrated, as shown in Figure 13.

As seen from Figure 13, no obvious changes can be seen from the numerical trends of the transverse acceleration and displacement of the conveyance, and the acceleration and displacement remained essentially constant as b increased. Comparing the response curves under the normal working conditions shown in Figure 7, there is little change. Therefore, it can be concluded that the gap between two adjacent steel guides has little effect on the responses of the transverse vibrations of the hoisting container.

3.4. Responses from Bending Deformation. Bending deformation is also a typical fault of the steel guide resulting from the long-time service of the machine. The form of bending deformation can be assumed as two ideal situations such as the inner and outer bending, as shown in Figure 14. Assuming that the bending was on the steel guide which is at the one side of the conveyance, and its deflection h was 0.01 m, 0.02 m, 0.03 m, 0.04 m, and 0.05 m. The bending fault of the steel guide cannot be directly set in Adams; hence, a bending steel guide with the deflection of 0.01 m, 0.02 m, 0.03 m, 0.04 m, and 0.05 m was first constructed in solid works and then imported into Adams to replace a normal

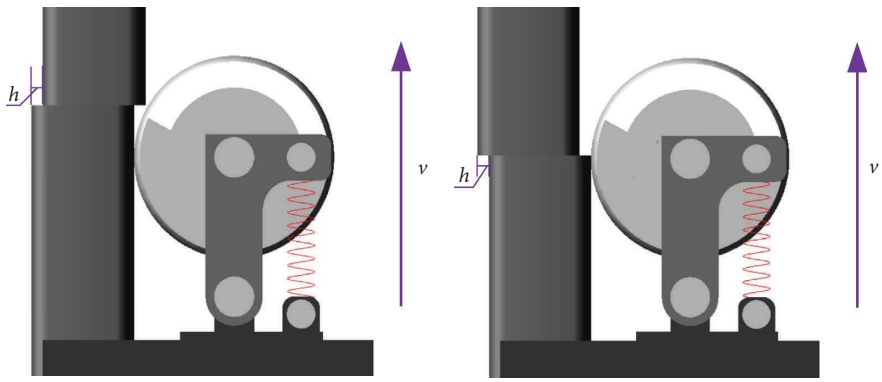

Figure 8: Interface misalignment settings. (a) Roll up to the step. (b) Roll down to the step.

one. When the conveyance was being hoisted through the inner and outer bending steel guides, the transverse accelerations and displacements of the conveyance were simulated and demonstrated, as shown in Figure 15.

As shown in Figures 15(a) and 15(b), after the guide roller had rolled onto the inner bending steel guide, continuous oscillations of the transverse vibration acceleration and displacement would be induced. Similarly, when the guide roller had rolled onto the outer bending steel guide, continuous oscillations of the transverse vibration acceleration and displacement would also be induced, as shown in Figures 15(c) and 15(d). As seen from the comparisons of the responses from the two fault situations, it can be concluded that the inner and outer bending deformations would result in the impact oscillations of the transverse vibrations of the hoisting conveyance, and the inner bending fault has a more serious effect on the transverse responses than the outer bending fault. The root cause is similar to two forms of interface misalignment failure. When the roller rolled onto the inner bending steel guide, it was obvious that the roller would be slowly squeezed by the guideway and then slowly returned to normal. Therefore, a vibration was excited first and then attenuated slowly. On the contrary, for the outer bending failure, the roller was not squeezed so that the spring would not be squeezed, so the whole process would only have a slight vibration.

For the first case, the amplitudes of both acceleration and displacement increased with h, while the frequencies of both remained constant. For the second case, the amplitude and frequency of both were not affected by h and were much smaller than those of the first case. In summary, the second case for the container vibration effect is negligible.

3.5. Responses from Orbital Tilt. As similar to the bending deformation of the steel guide, orbital tilt which makes the steel guide deflect as a whole is also a guide fault resulting from the long-time service of the machine. The form of orbital tilt can be assumed as two ideal situations such as the inner and outer tilt, as shown in Figure 16. Assuming that the tilt was on the steel guide which is at the one side of the conveyance, and its deflection h was 0.01 m, 0.02 m, 0.03 m, 0.04 m, and 0.05 m. When the conveyance was being hoisted through the inner and outer tilt steel guides, the transverse accelerations and displacements of the conveyance were simulated and demonstrated, as shown in Figure 17.

As shown in Figures 17(a) and 17(b), after the guide roller had rolled onto the inner tilt steel guide, continuous oscillations of the transverse vibration acceleration and displacement would be induced, and the amplitude increased as h increased. However, as seen in Figures 17(c) and 17(d), the outer tilt of the steel guide has little effect on the transverse response of the conveyance. Hence, it can be concluded that the effect of the inner tilt fault on the transverse vibrations of the hoisting conveyance cannot be ignored, while the effect from the outer tilt fault can be ignored.

3.6. Vibration Responses under the Action of Multiple Faults. This section would further discuss the case of one-to-one coupling of several faults that have a large impact on conveyance vibration. Since the vibration response curves for bending deformation and orbital tilt are similar, only the case where step, bulge, and bend were coupled one-to-one was considered. The specific coupling fault forms are shown in Figure 18. The height of the step and bulge as well as the deflection of the bending deformation was chosen to have a greater impact on the container, i.e., 5 cm.

As seen from the two plots in Figures 19(a) and 19(b), both cases in Figure 18(a) excite four peak accelerations. The Δt_1 in both figures is the same, which represents the time difference between the upper and lower rollers which fixed on the container passing through the fault; Δt_2 is determined by the distance between the two faults, and the further the distance is, the larger the Δt_2 is, and the fault distances of 3 m and 15 m were selected in Figure 18(a), respectively. As can be seen from the two graphs in Figures 19(c) and 19(d), the two cases in Figure 18(a) had almost the same effect on the displacement, and both of the final displacements stabilized at a value rather than becoming zero.

The situation in the two panels of Figures 20(a) and 20(b) is similar to that of Figures 19(a) and 19(b), which also excited four acceleration peaks, and the meanings of Δt_1 and

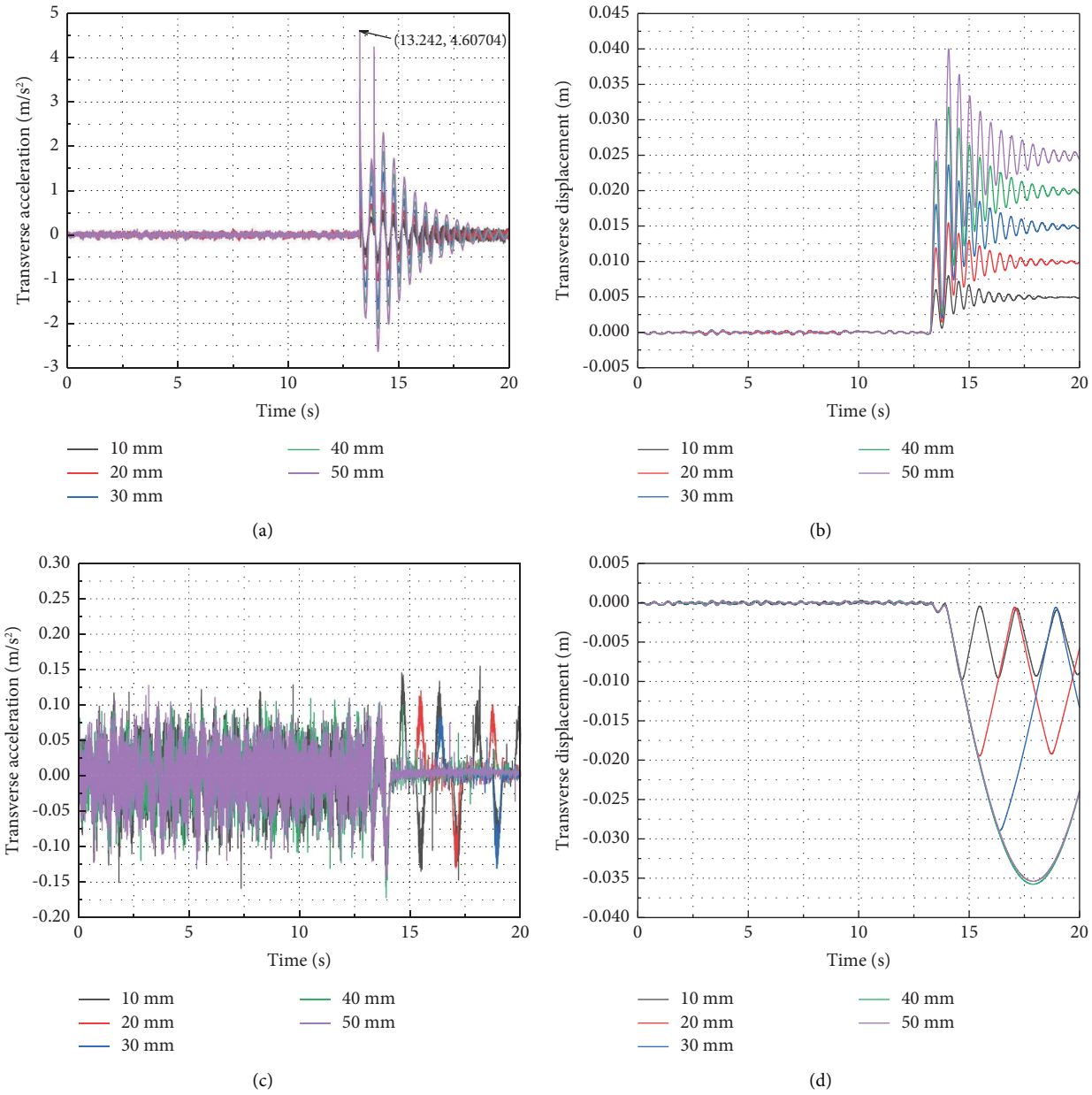

FIGURE 9: Transverse vibration responses of conveyance excited by interface misalignment: (a) transverse acceleration when rolling up to the step; (b) transverse displacement when rolling up to the step; (c) transverse acceleration when rolling down to the step; (d) transverse displacement when rolling down to the step.

Δt_2 are the same. The circled part in Figure 20(d) was due to the long distance between the bulge and the step, and the displacement of the container was excited after the container passed through the bulge, and then the container subsequently passed through the step. Whereas, in Figure 20(c), the displacement was affected close to the effect of a coupling due to the close distance between the two faults.

From Figures 21 and 22, it can be seen that when the step and bending deformation faults were coupled, the accelerations and displacements excited by them were coupled accordingly and characterized clearly, and the coupled faults had a large impact on the conveyance.

Comparing Figure 23 with Figures 11, 15(a), and 15(b), it can be seen that when a bulge was present on the bending guide, the bulge played a major role in influencing the acceleration, while the curved guide played a dominant role in the displacement.

As can be seen in Figures 24 and 25, the effect of bulge and bending deformation coupling on acceleration is similar to that in Figure 21, while the effect on displacement came mainly from the bending guideway. The circled portion in Figure 24(d) was excited by the bulge, but not in Figures 24(c), 25(c), and 25(d). It can be seen that when the container passed through the bending

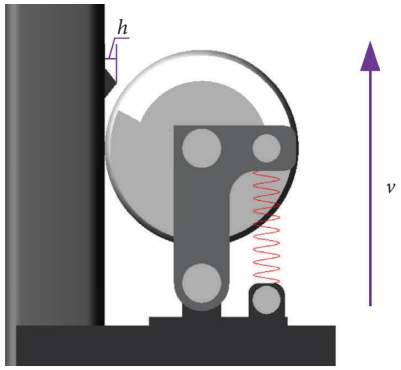

Figure 10: Local bulge setting.

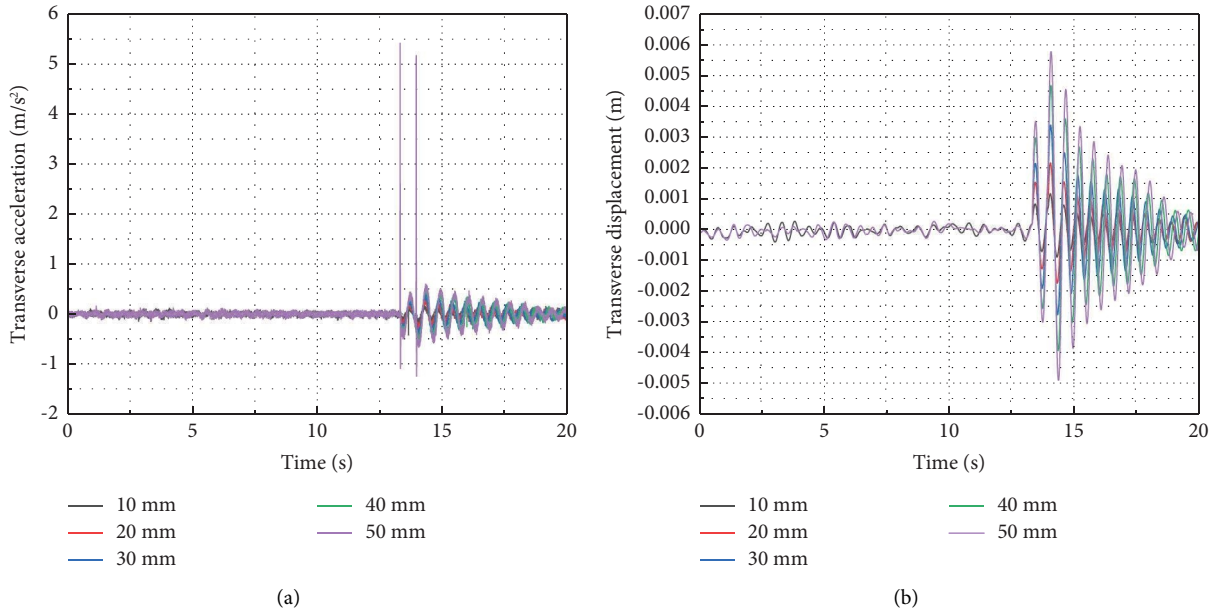

Figure 11: Transverse vibration response of conveyance under local bulge: (a) transverse acceleration; (b) transverse displacement.

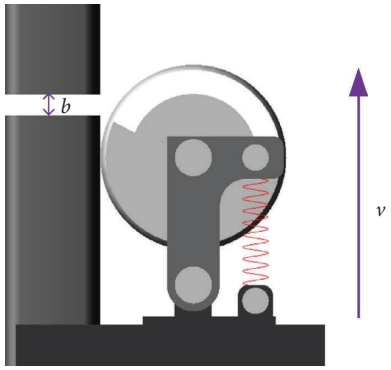

Figure 12: Orbital gap setting.

guide before passing through the bulge, the bulge did not have an effect on the displacement; when the container passed through the bulge before passing through the bending guide, the bulge excited an insignificant effect if the two were close together and a significant effect if they were farther apart, but it was much smaller compared to the displacement excited by the subsequent bending guide.

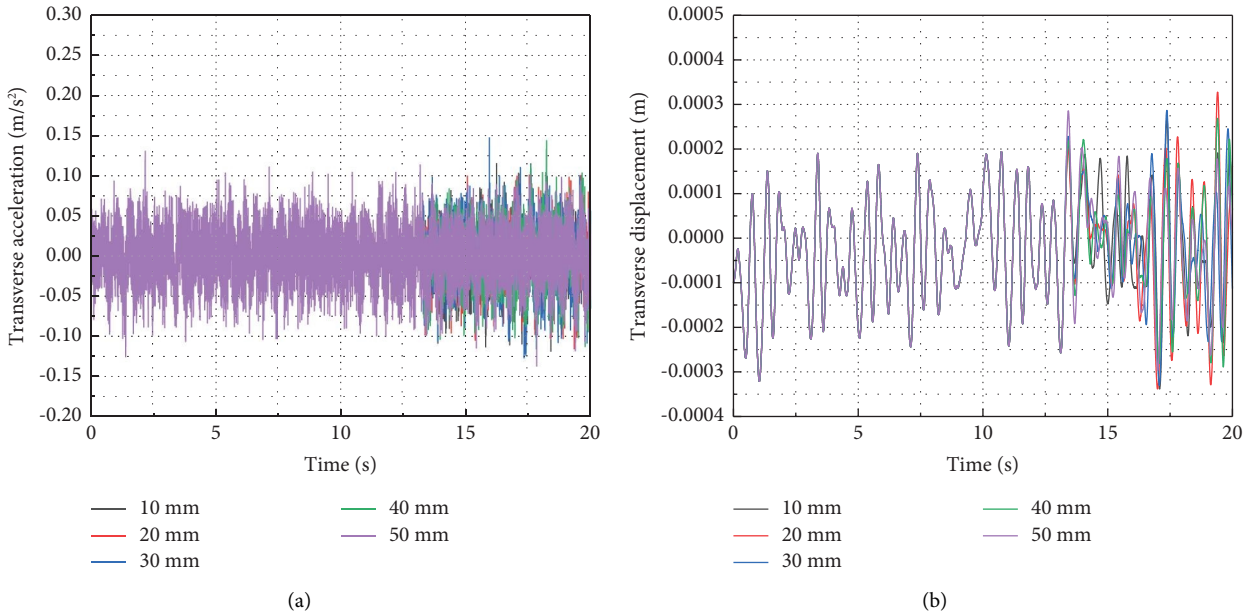

Figure 13: Transverse vibration response of conveyance under orbital gap: (a) transverse acceleration; (b) transverse displacement.

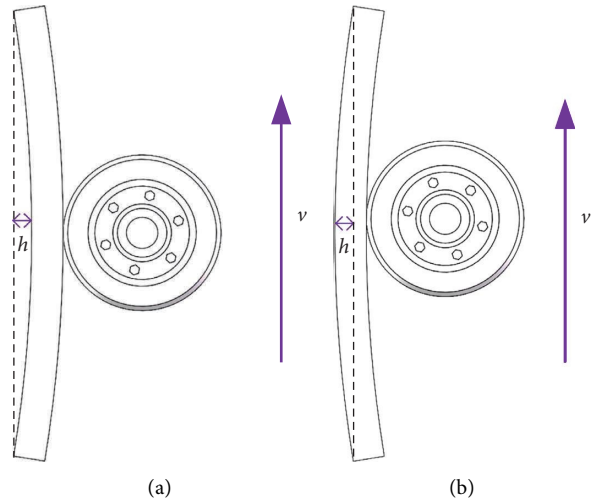

Figure 14: Bending deformation settings: (a) inner bending; (b) outer bending.

3.7. Synthetic Analysis. From the above simulations and analyses, it can be seen that the gap between two adjacent steel guides has little effect on the responses of the transverse vibrations of the hoisting container, but the other four failure modes mentioned in Figure 2 can excite the transverse vibrations of the container with different strengths. Also, the interface misalignment and local bulge would contribute to a more serious vibration compared to the situations of guide bending and tilt. Also, coupling faults between them can lead to severe vibration.

By comparing the transverse vibration displacements to the corresponding accelerations from each situation, it can be seen that the amplitudes of the oscillating displacements are so small that they can be ignored. However, the impact resulting from the oscillating accelerations cannot be ignored. For example, the impact acceleration from the interface misalignment in Figure 9(a) has a maximum value of 4.60704 m/s^2 and would last for a period of time. The hoisting mass is 34 t. Therefore, an oscillating impact force with a peak value of 156639.36 N would be synchronously induced, which will lead to fatigue damage of the machine and accelerate the damage of the corresponding equipment, seriously reducing the reliability of the machine and the safety of coal production.

Therefore, a method to reduce the shock acceleration should be proposed.

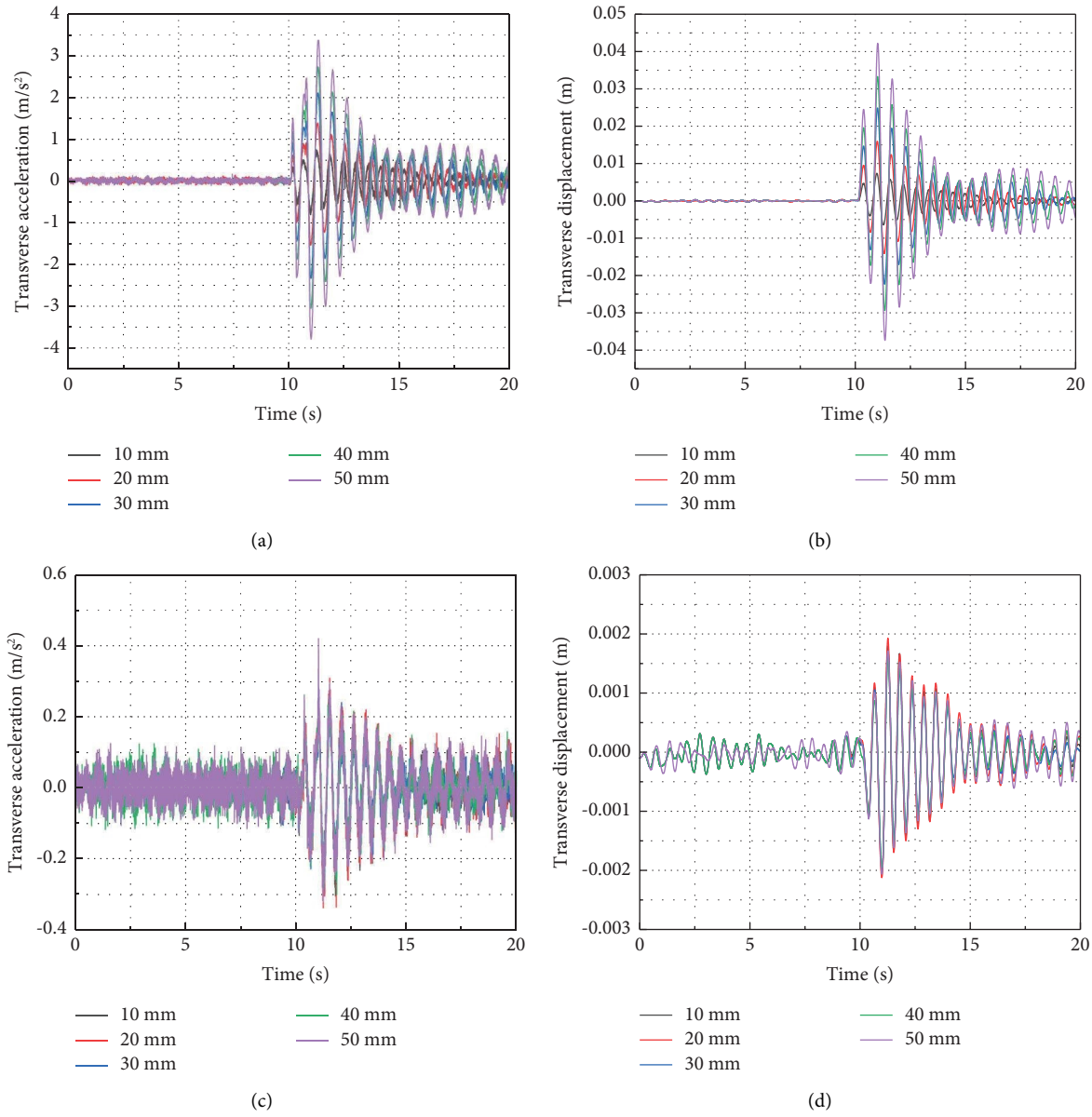

Figure 15: Transverse vibration response of conveyance under bending deformation: (a) transverse acceleration from the inner bending; (b) transverse displacement from the inner bending; (c) transverse acceleration from the outer bending; (d) transverse displacement from the outer bending.

4. Vibration Control of Semiactive with MR Damper

4.1. New Roller Cage Shoe with MR Damper. At present, mine hoisting systems still adopt the traditional roller cage shoes and have not been equipped with a reliable vibration reduction device and provided with an effective vibration reduction method, so the intense vibration was more easily excited. An innovative structural form of a roller cage shoe equipped with an MR damper, as shown in Figure 26, was proposed to decrease the impact responses of the hoisting conveyance caused by various failures of the rigid guides. The structure is not a simple passive structure, and the damping force can be adjusted in real time to achieve the effect of vibration control. Compared with the hydraulic cylinder, it has fast response, fast damping force adjustment, and is easy to be used for vibration control. The MR damper is a semiactive control device with a simple structure that is lightweight. Compared with active control, it will not damage the stability of the system. The arrangement of the MR damper in the roller cage shoe is at an angle of 60 degrees to the base, providing a better transverse vibration reduction than the conventional device that is vertical. The damping force provided by the MR damper could be decomposed into a horizontal component and a vertical component, and the horizontal MR damping force could be adjusted.

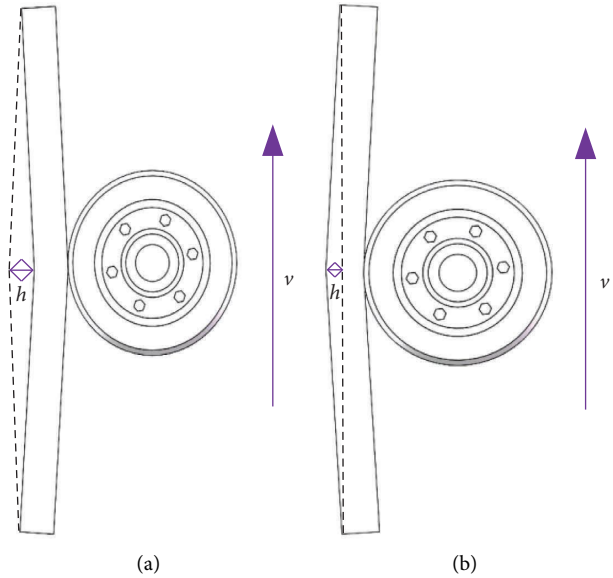

Figure 16: Orbital tilt settings: (a) inner tilt; (b) outer tilt.

A MR damper is filled with a magnetorheological fluid controlled by a magnetic field. The main feature of a MR damper is that when there is no applied magnetic field, the magnetorheological fluid is a free-flowing liquid; under the action of the external magnetic field, the MR fluid will instantly change from a liquid to a semisolid, and when the magnetic field reaches a certain strength, it will completely become solid. This liquid-solid transition is fast and reversible and can be accomplished in milliseconds. The damping force can be adjusted in real time by applying a small control current to the MR damper.

4.2. Overall Control Process. In order to reduce the transverse vibration of the container, two semiactive control strategies, PID and fuzzy PID methods, were proposed in this paper. Moreover, Adams and MATLAB/Simulink cosimulation were used to test the performance of these two semiactive control strategies. The required input and output variables were first established in Adams, and then the virtual prototype model was exported from Adams to the Simulink environment of MATLAB, represented by the "adams_sub" module. Finally, the semiactive controller was established in Simulink. After the simulation, the Adams model would automatically switch off and return to Simulink, where the output from the joint simulation could be observed.

Since the roller cage shoes are connected to the hoisting conveyance, controlling the transverse vibration of the container can be simplified to controlling the vibration of the four bases of the roller cage shoes. First, the real-time transverse accelerations of the four bases of the roller cage shoes and the displacements and velocities of the damper pistons were input to the controller. Subsequently, the controller calculates the desired damping force according to the acceleration obtained and its derivative. Then, the desired control current was calculated from the hyperbolic tangent inverse model. The MR damper used in this paper has a minimum input current of 0 A and the maximum input current of 1 A. When the direction of the desired control force is different from the direction of the damping force of the damper, the MR damper coil current should be taken as 0 A. If the fuzzy PID controller expects a control current between 0 and 1 A, the coil current of the damper is equal to the control current. And if the desired control current of the fuzzy PID controller is higher than 1A, the coil current of the damper is the maximum value of 1 A. Finally, the obtained currents were brought into the hyperbolic tangent model to obtain the damping forces and then input into Adams to complete the vibration control. The control idea is shown in the dynamics model in Figure 27. The control principle is shown in Figure 28, since the four damping forces were calculated by the same process, only one of them is given in the figure.

In the diagram, m_c is the mass of the container; m_r is the mass of the roller cage shoe; k_r is the contact rigidity between the roller and the rigid guide; k_s is the cushioning stiffness of the roller cage shoe; c is the cushioning damping of the roller cage shoe; a_c is the transverse acceleration of the container; x_c is the transverse displacement of the container; $f_1 \sim f_4$ are the horizontal components of the damping forces; and $a_1 \sim a_4$ are the transverse accelerations of the roller cage shoes.

The hyperbolic tangent model of the MR damper has been proposed by previous scholars [33], which was in good agreement with the experimental results and could be effectively used for semiactive control in this paper. The model was given by

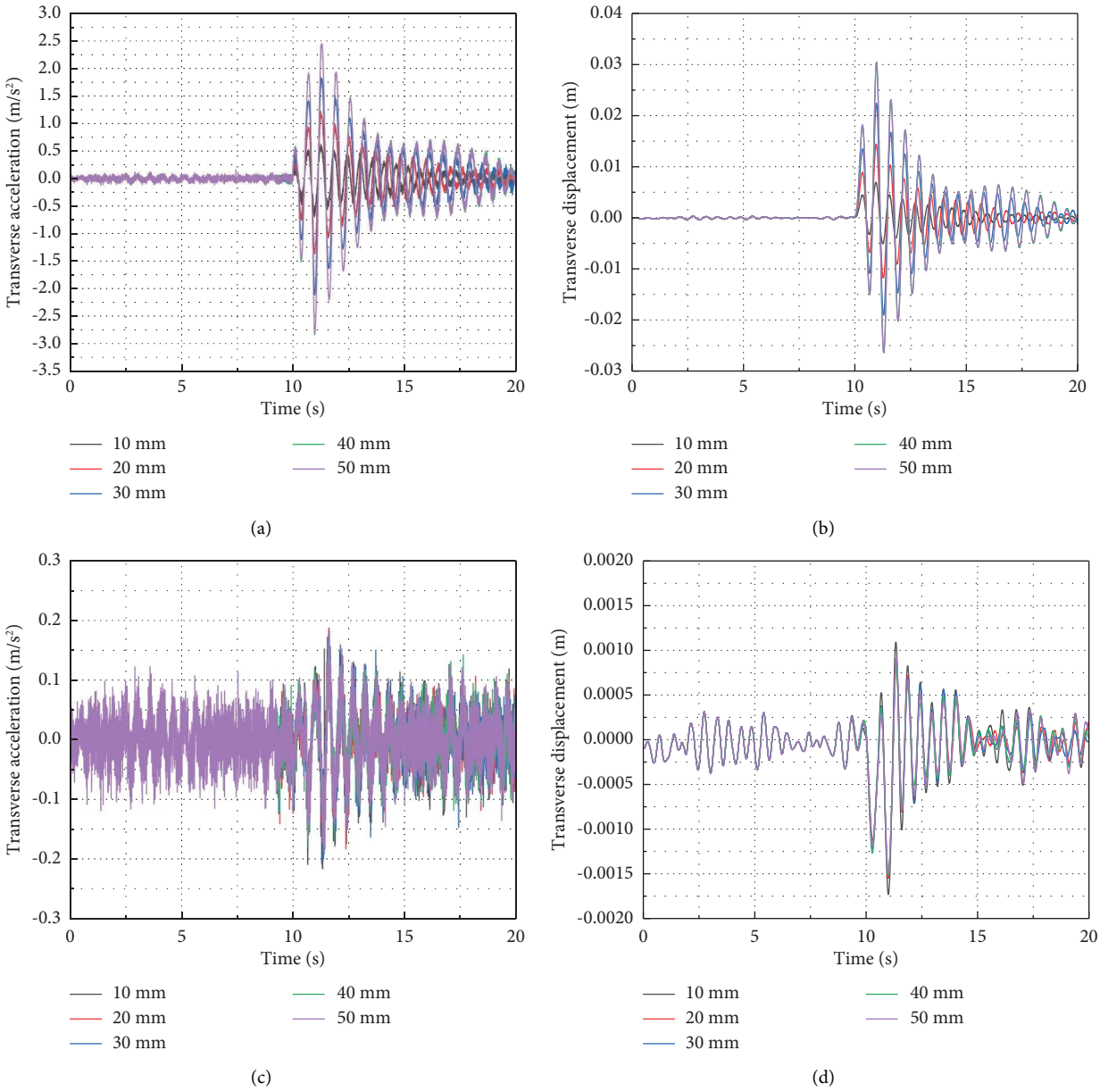

Figure 17: Transverse vibration response of conveyance under orbital tilt: (a) transverse acceleration from the inner tilt; (b) transverse displacement from the inner tilt; (c) transverse acceleration from the outer tilt; (d) transverse displacement from the outer tilt.

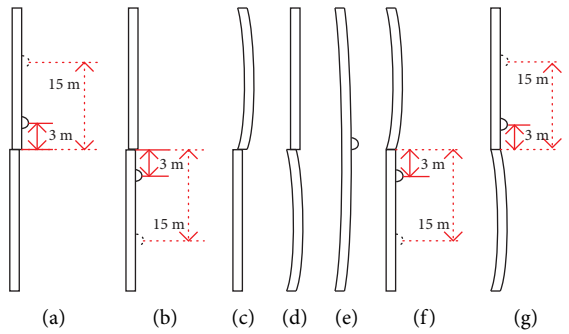

Figure 18: Coupling faults.

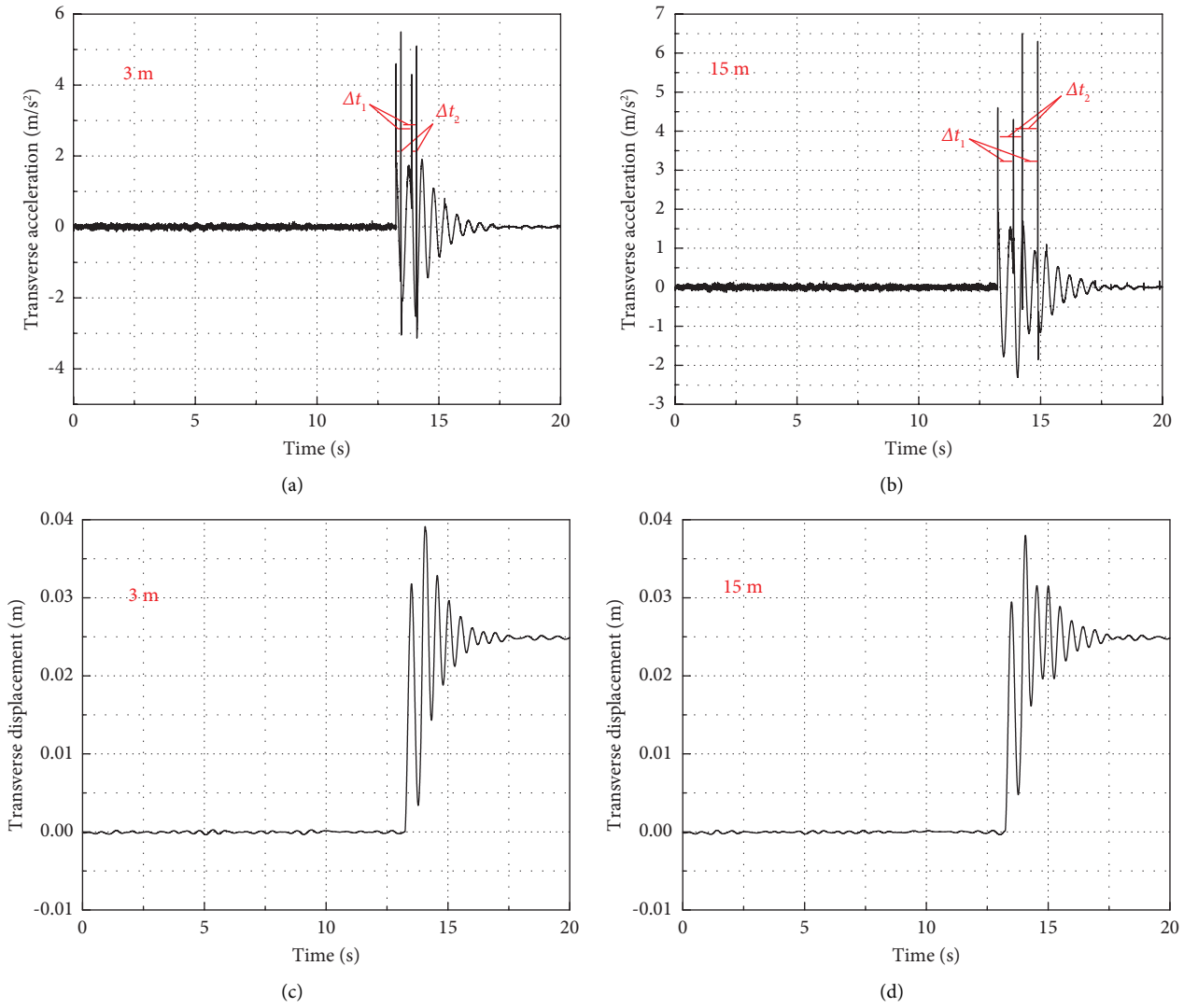

Figure 19: Acceleration and displacement for two different cases of (a) failure in Figure 18.

$$f = a_{11}\text{tsnh}\left(776.5809\left(x + 0.3506x\right)\right) + a_3\left(x + 0.3506x\right) + 7.1671. \tag{5}$$

In the following equation:

$$\begin{cases} a_1 = 117.26107I + 40.4957, \\ a_3 = 484.3815I + 167.2799. \end{cases} \tag{6}$$

Its inverse model can be derived as follows:

$$I = \frac{f - 7.1671 - (40.4957m + 167.2799n)}{117.2610m + 484.3815n}. \tag{7}$$

In the following equation:

$$m = \tanh\left[776.5809\left(x + 0.3506x\right)\right], n = x + 0.3506x, \tag{8}$$

where f is the damping force; I is the current; and x and $\dot{x}$ are the displacement and velocity of the magnetorheological damper piston, respectively.

4.3. Semiactive Controller Design. The formula for the traditional PID controller is as follows:

$$u(t) = K_p e(t) + K_i \int_0^t e(t)dt + K_d \frac{de(t)}{d(t)}, \tag{9}$$

where K_p is the proportional gain; K_i is the integral gain; K_d is the differential gain; $e(t)$ is the input for the PID controller, i.e., the deviation between the acceleration of base and zero acceleration; and $u(t)$ is the output for the PID controller, the required damping force.

Because the parameters of traditional PID controllers cannot be changed in real time as the system runs, the control of the PID controllers is limited. To better suppress the transverse vibration of the hoisting container, this paper proposed a fuzzy PID control strategy.

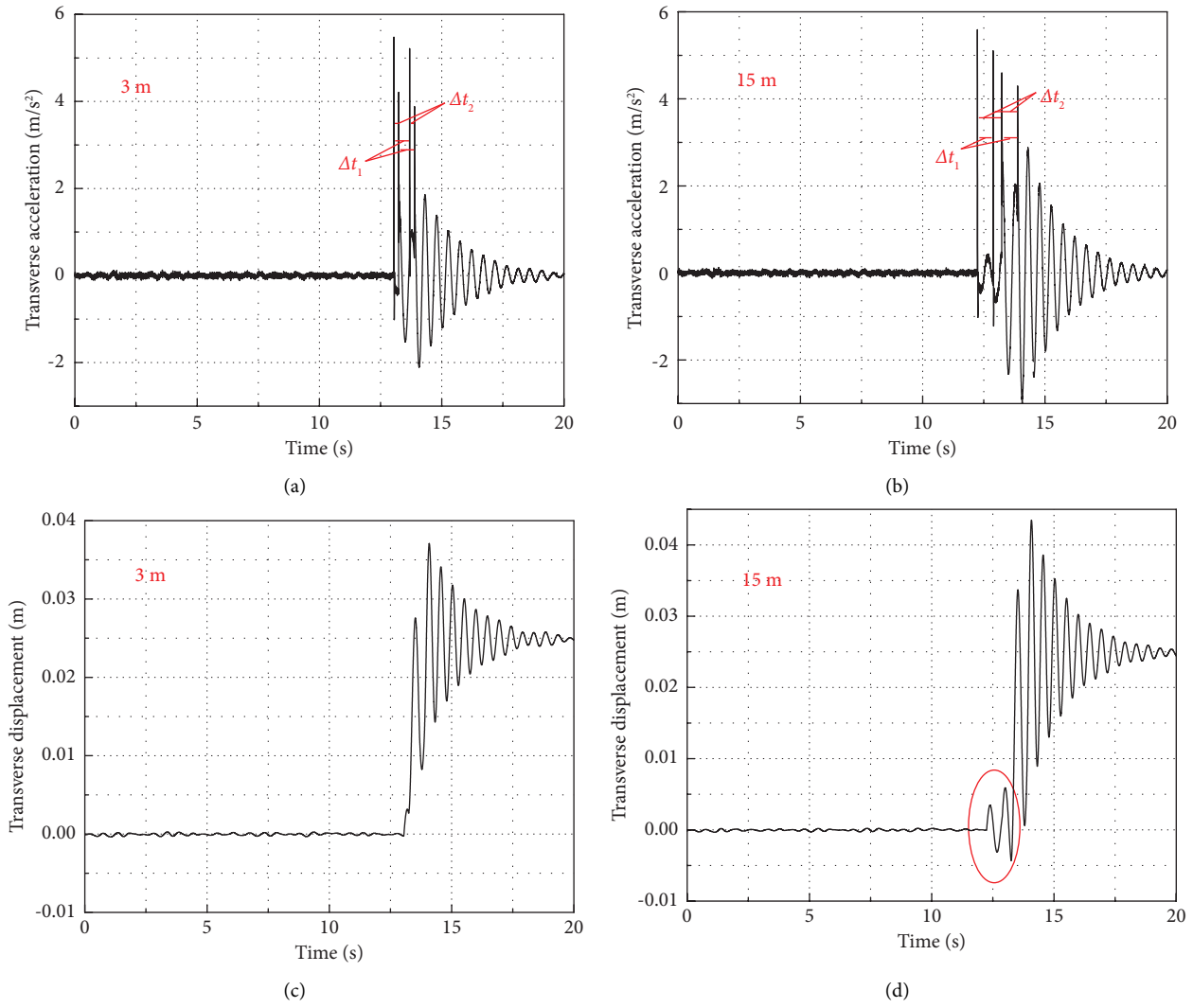

Figure 20: Acceleration and displacement for two different cases of (b) failure in Figure 18.

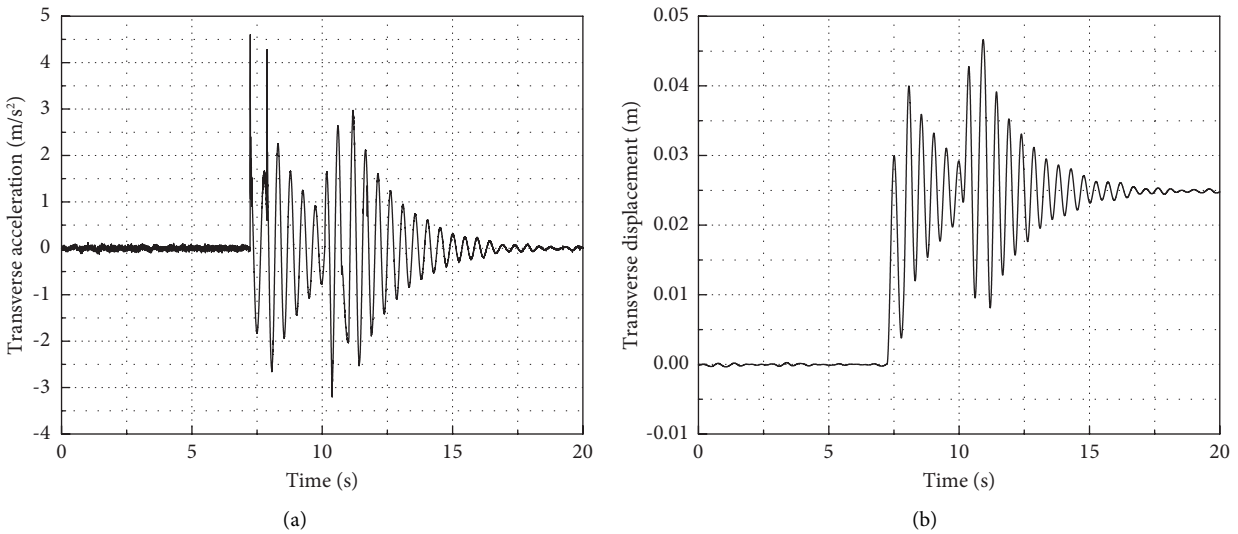

Figure 21: Acceleration and displacement of (c) failure in Figure 18.

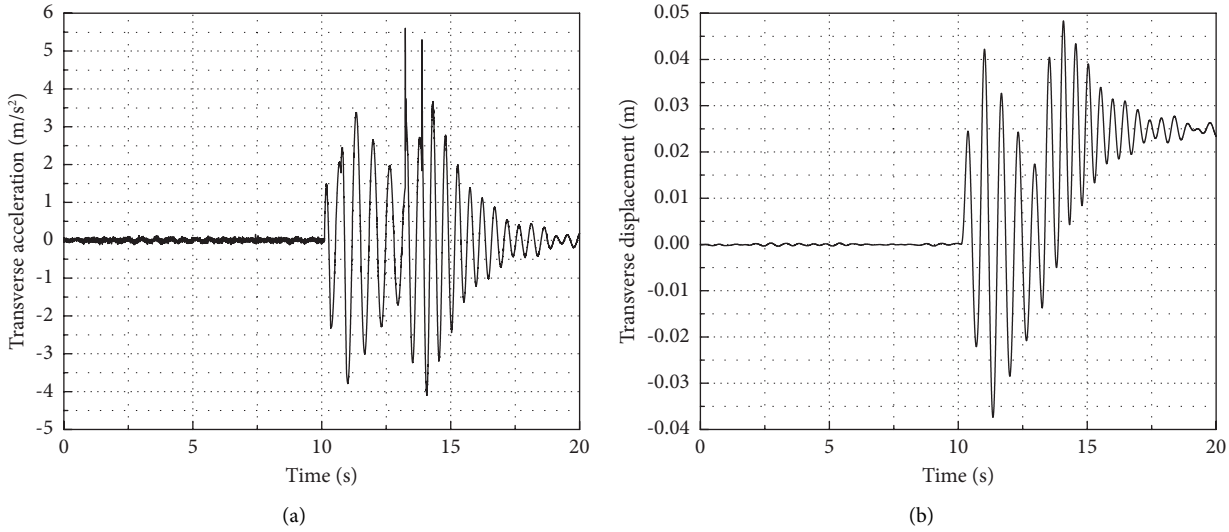

Figure 22: Acceleration and displacement of (d) failure in Figure 18.

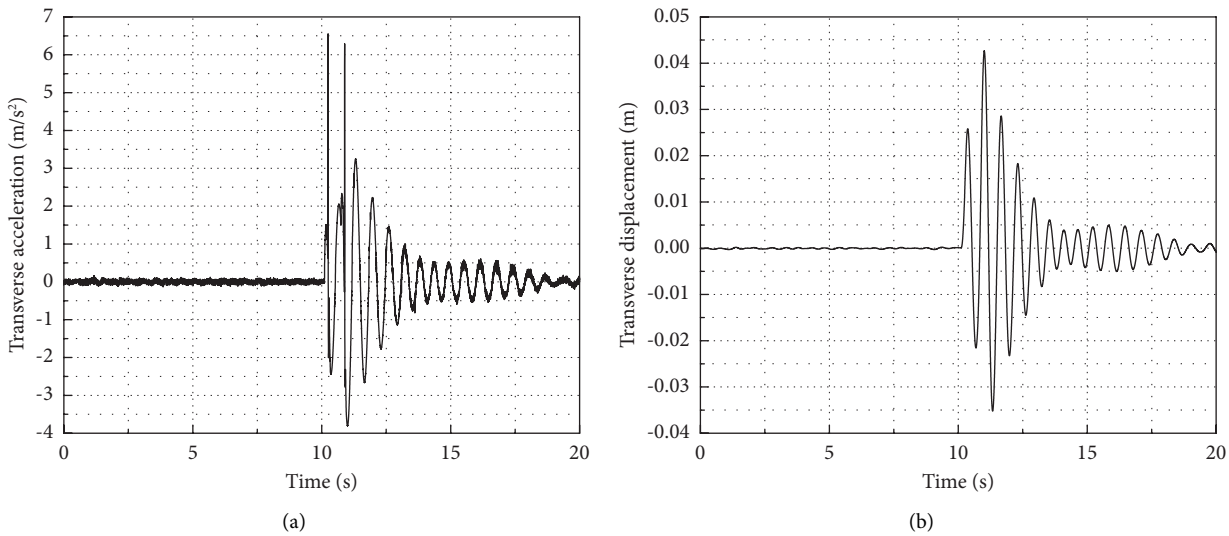

Figure 23: Acceleration and displacement of (e) failure in Figure 18.

The control principle of the fuzzy PID controller is to analyze the input signals of the PID controller through the fuzzy algorithm and then change the parameters in real time. The fuzzy PID control algorithm can be represented as follows:

$$u(t) = \left(K_{p0} + \Delta K_p \times q_p\right)e(t) + \left(K_{i0} + \Delta K_i \times q_i\right)\int_0^t e(t)dt + \left(K_{d0} + \Delta K_d \times q_d\right)\frac{de(t)}{d(t)}, \tag{10}$$

where K_{p0}, K_{i0}, and K_{d0} are the initial parameters for the PID controller; ΔK_p, ΔK_i, and ΔK_d are the output variables for the fuzzy controller; q_p, q_i and q_d are the output scaling gains in the fuzzy controller; $e(t)$ is the input for the fuzzy PID controller, i.e., the deviation between the acceleration of base and zero acceleration; and $u(t)$ is the output for the fuzzy PID controller, the desired damping force.

The crucial point to designing a fuzzy PID controller is to calculate ΔK_p, ΔK_i, and ΔK_d. The inputs to the fuzzy controller are the vibration acceleration deviation of the base and its derivative. ΔK_p, ΔK_i, and ΔK_d are the outputs of the fuzzy controller. The working principle of the fuzzy PID control is shown in Figure 29.

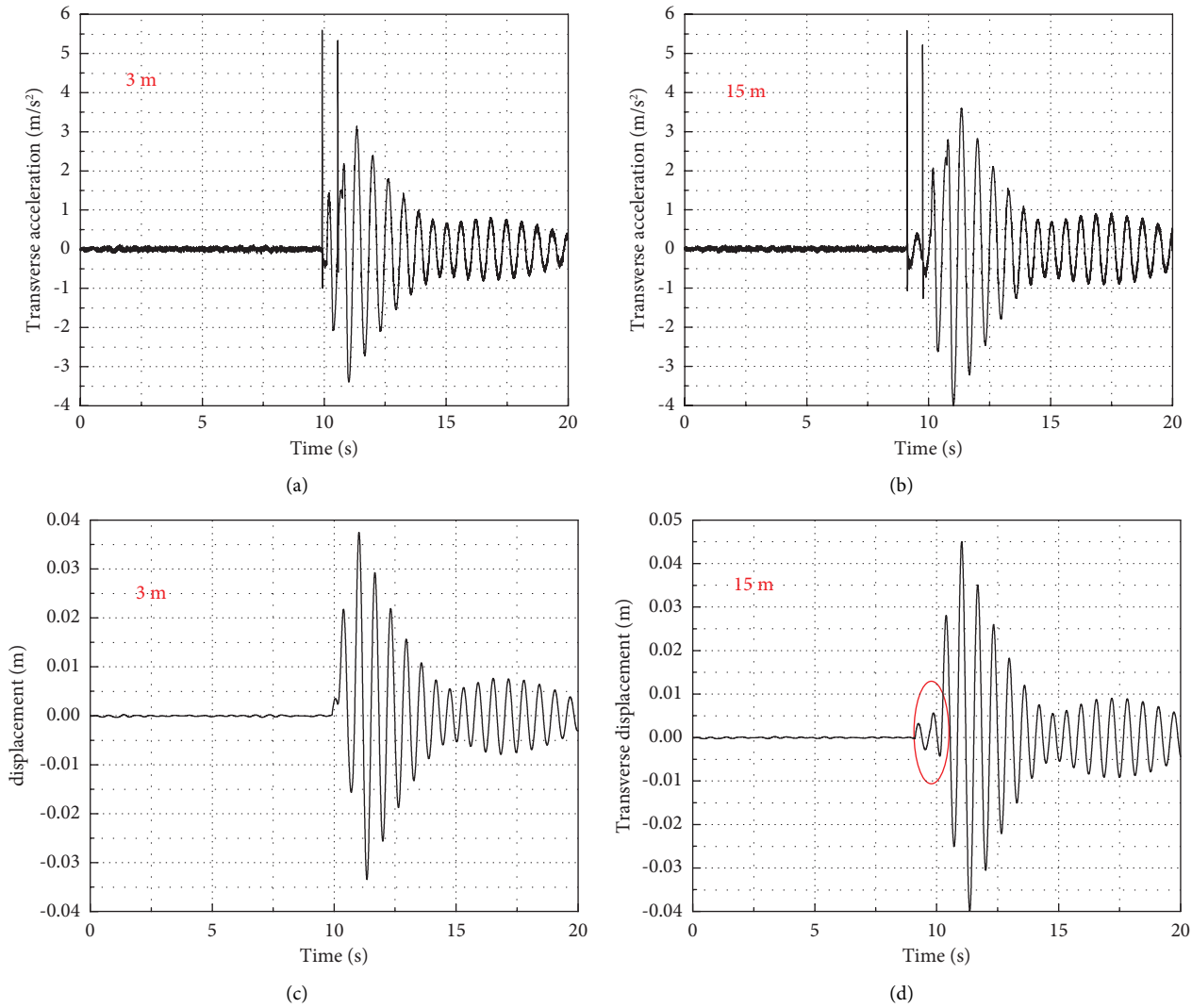

Figure 24: Acceleration and displacement for two different cases of (f) failure in Figure 18.

The input signals were divided into seven options through the fuzzy algorithm in the fuzzy PID controller. The algorithm first fuzzed the deviation signal and its derivatives into fuzzy variables. Subsequently, the fuzzy inference machine containing fuzzy rules received the fuzzy variable. Then, the fuzzy inference machine calculated the fuzzy results using the fuzzy algorithm. Finally, the fuzzy results were antiblurred into the variation values of proportional, integral, and differential parameters.

Mamdani method was selected as a fuzzy inference method in this study. This fuzzy control algorithm used the Gaussian affiliation function as the affiliation function. Both the acceleration deviation of the base and its derivative were divided into seven fuzzy subsets. The fuzzy subsets of both the acceleration deviation and its derivative were denoted as {NB, NM, NS, ZE, PS, PM, and PB}. Also, the fuzzy subsets represent negative large, negative medium, negative small, zero, positive small, positive medium, and positive large, respectively. The universe of discourse for the acceleration deviation $e(t)$ was taken as {−6, −4, −2, 0, 2, 4, and 6}. Also, the universe of discourse for the derivative of the acceleration deviation $de(t)/dt$ was taken as {−20, −40/3, −20/3, 0, 20/3, 40/3, and 20}. The proportional, integral and differential parameters were all divided into eight fuzzy subsets. Their fuzzy subsets were all denoted as {NB, NM, NS, ZN, ZP, PS, PM, and PB}. Also, the universes of discourse for the proportional, integral, and differential parameters were {0, 25/7, 50/7, 75/7, 100/7, 125/7, 150/7, and 25}, {0, 30/7, 60/7, 90/7, 120/7, 150/7, 180/7, and 30}, and {0, 35/7, 70/7, 105/7, 140/7, 175/7, 210/7, and 35}, respectively. The related membership function diagrams of the input and output variables are shown in Figure 30.

Fuzzy rules are mainly established by practical experience combined with specific problems. As an example, if the acceleration deviation $e(t)$ is large, the transverse acceleration of the container is far from the reference value. At the same time, a smaller derivative of the acceleration deviation $de(t)/dt$ indicates that the acceleration of the container is slowly approaching the reference value. The real-time acceleration is relatively large at this time. Therefore, the

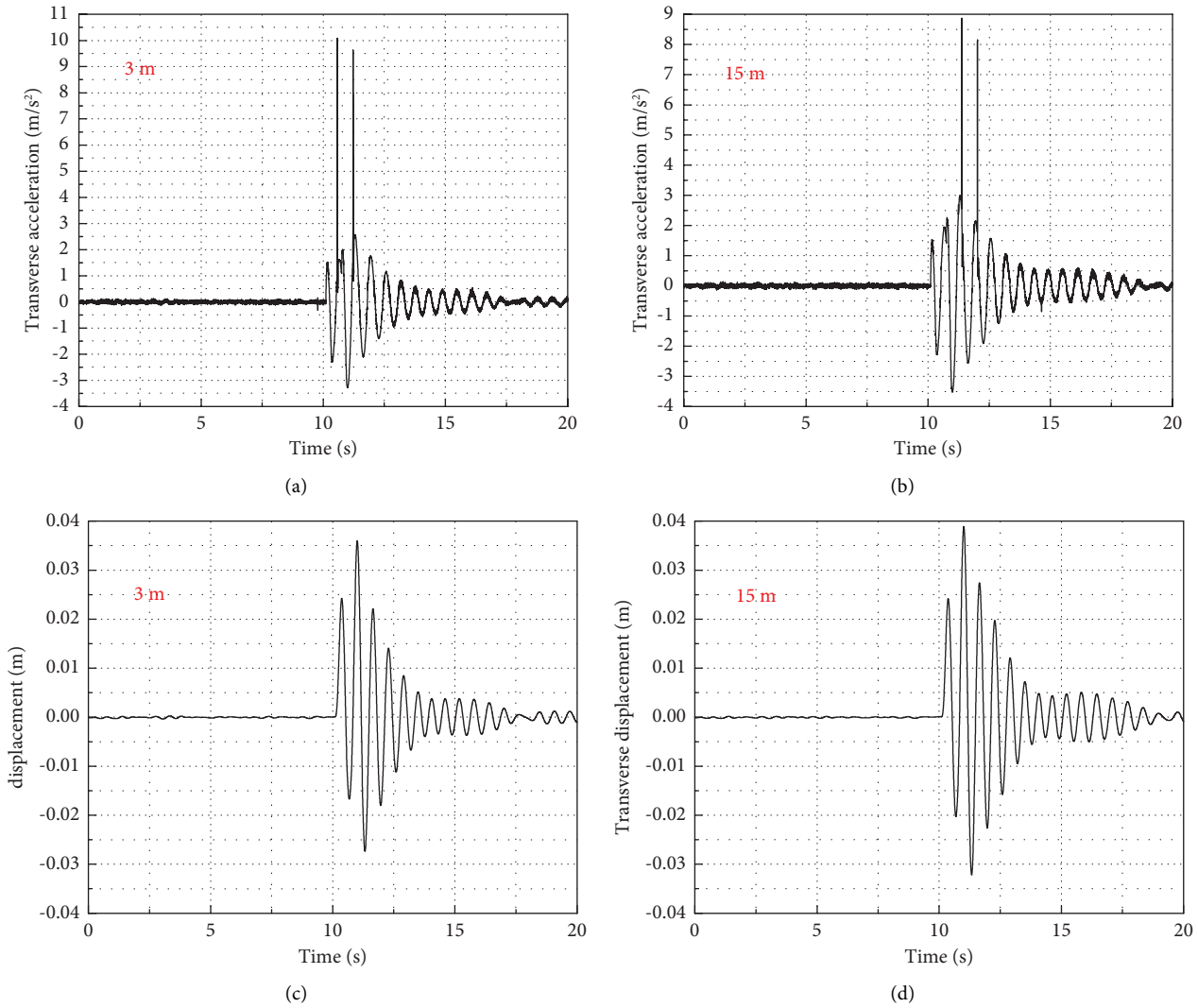

Figure 25: Acceleration and displacement for two different cases of (g) failure in Figure 18.

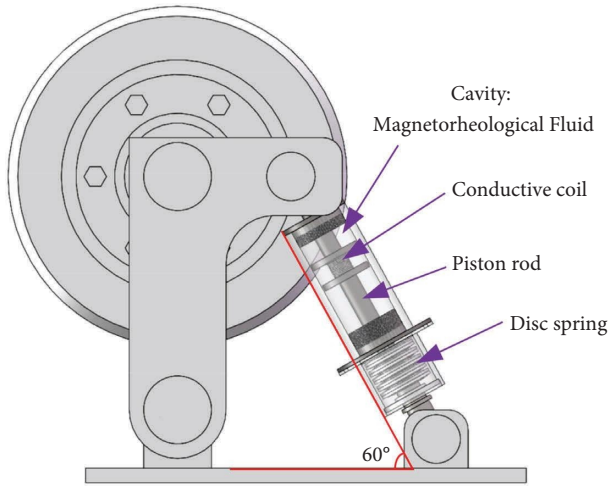

Figure 26: New roller cage shoe with MR damper.

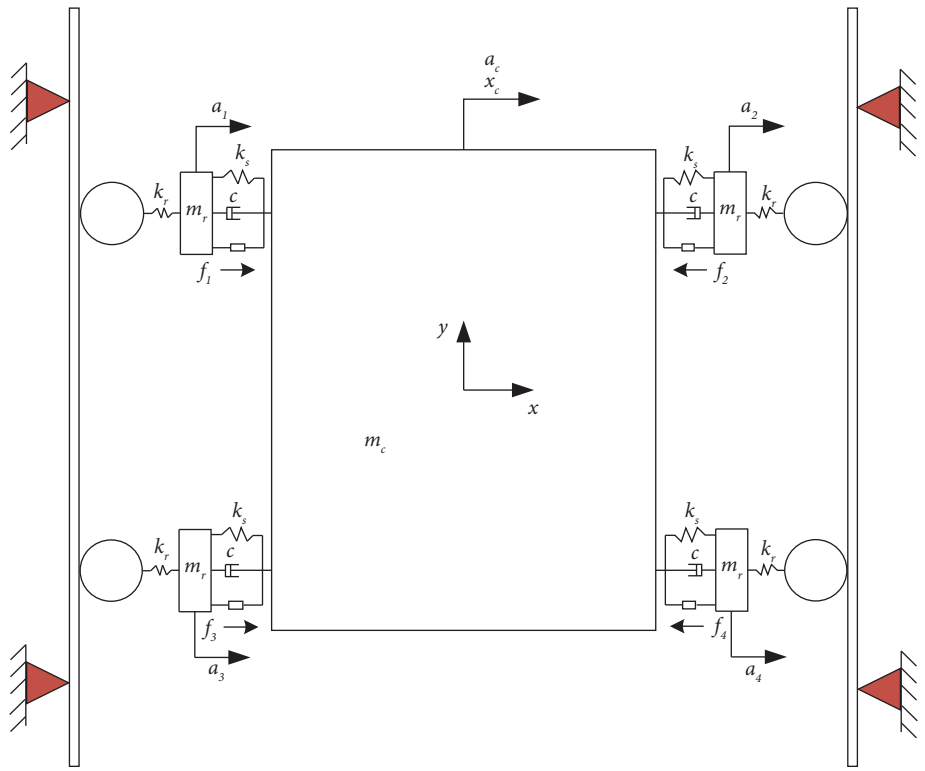

Figure 27: Dynamic model of container.

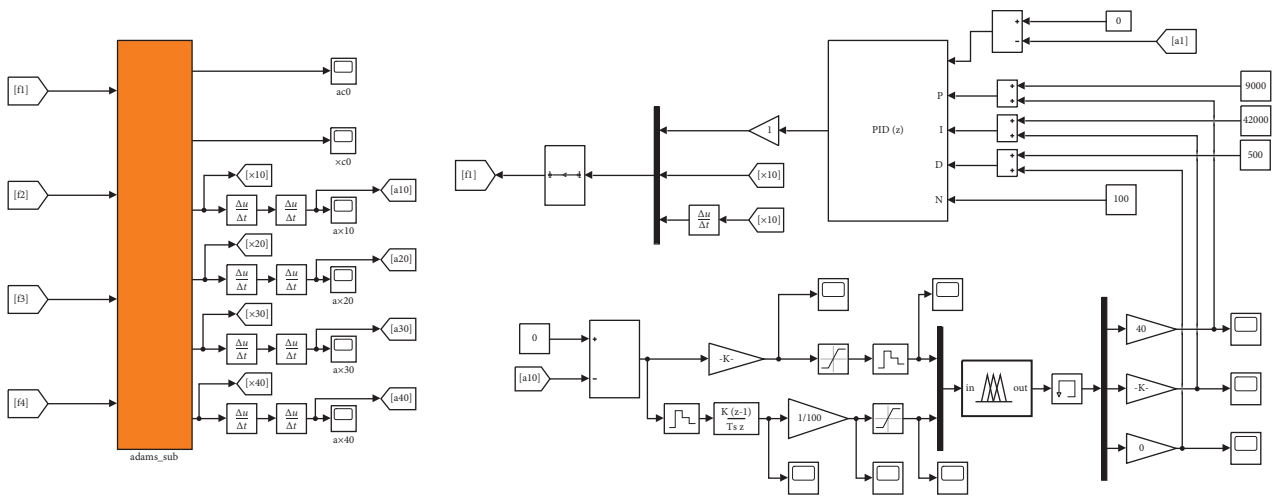

Figure 28: Control schematic diagram.

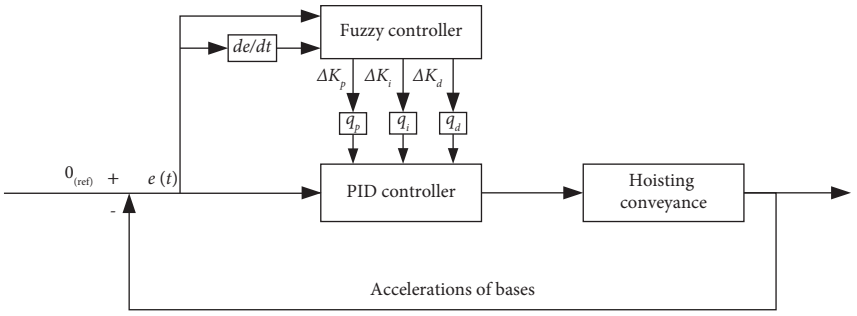

Figure 29: Fuzzy PID controller scheme.

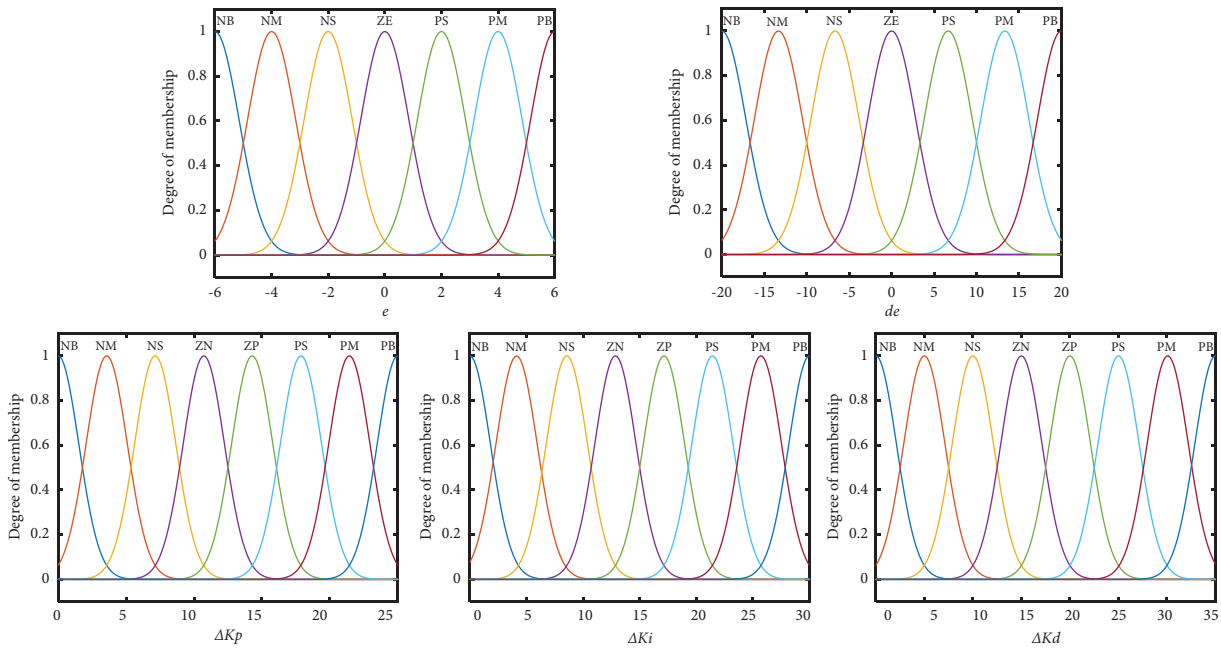

Figure 30: Membership function diagrams of the input and output variables.

controller's output should be a large value opposite to the acceleration symbol, so that the acceleration can be quickly closed to the reference value to reduce the vibration. Furthermore, the centroid method was used for defuzzification to get the output values in the fuzzy controller. The fuzzy rules for ΔK_p, ΔK_i, and ΔK_d are shown in Tables 4–6, and the three-dimensional surface of the fuzzy rules is shown in Figure 31.

4.4. Joint Simulation Analysis. Since interface misalignment, local bulge, guideway bending, and tilting all excite vibration of the container, and the bending and tilting situations are similar enough to be grouped together, a simple vibration suppression discussion of the above three faults was carried out in this chapter, and the transverse acceleration and displacement of the container were taken as evaluation indexes of the vibration reduction effect. Compare different controllers, including PID controller, fuzzy PID controller, and passive condition (i.e., input control current is 0 A). The completed model in Chapter 2 was used, and the excitation was the same as that in Chapter 3. In order to improve the precision of joint simulation, the simulation step was set to 0.001 in Simulink. The comparison of transverse vibration responses of the container under step excitation by joint simulation is shown in Figure 32.

As seen from Figure 32, under both control strategies, the amplitude and frequency of acceleration and displacement under the three typical faults were improved to some extent, and the control effect of fuzzy PID is better than that of PID. The root mean square (RMS) and the maximum value (Max) calculations of accelerations for the three faults are shown in Tables 7–9. The RMS of acceleration represents the magnitude of vibration and the density of impact, which can effectively reflect the effect of vibration suppression.

Table 4: Rule base for variable ΔK_p.

ΔK_p		*de*						
		NB	NM	NS	ZE	PS	PM	PB
e	NB	NB	NB	NM	ZN	ZP	PS	PM
	NM	NM	NM	NS	ZN	ZN	ZP	ZP
	NS	NB	NB	NM	ZN	ZP	PS	PS
	ZE	NS	ZN	ZP	ZP	PS	PS	PS
	PS	NS	ZN	ZN	ZP	PS	PS	PM
	PM	ZN	ZN	ZN	ZP	ZP	ZP	PS
	PB	NM	NS	ZN	ZP	PS	PM	PB

Table 5: Rule base for variable ΔK_i.

ΔK_i		*de*						
		NB	NM	NS	ZE	PS	PM	PB
e	NB	NB	NB	NM	ZN	ZN	PS	PS
	NM	NM	NS	NS	ZN	ZP	PS	PM
	NS	NB	NM	NS	ZN	ZP	ZP	PS
	ZE	NS	ZN	ZP	ZP	PS	PS	PM
	PS	ZN	ZP	ZP	ZP	PS	PS	PM
	PM	ZN	ZP	ZP	ZP	PS	PS	PS
	PB	NM	NS	ZN	ZP	PS	PM	PB

Table 6: Rule base for variable ΔK_d.

ΔK_d		*de*						
		NB	NM	NS	ZE	PS	PM	PB
e	NB	NB	NM	NM	ZN	ZN	PS	PS
	NM	NM	NM	NS	NS	ZP	ZP	PS
	NS	NB	NM	NM	NS	ZP	ZP	PS
	ZE	NS	NS	NS	ZN	ZN	ZP	PS
	PS	NS	NS	ZP	ZP	ZP	PS	PS
	PM	ZN	ZN	ZP	ZP	ZP	PS	PS
	PB	NM	NS	ZN	ZP	PS	PM	PB

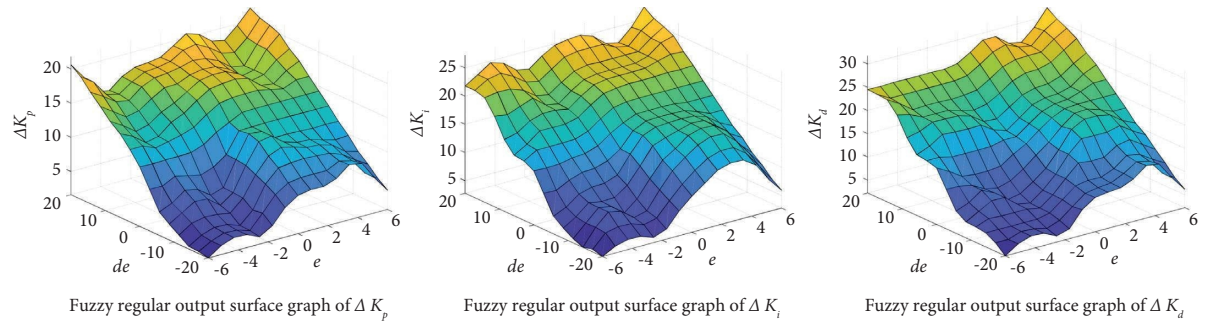

Fuzzy regular output surface graph of ΔK_p Fuzzy regular output surface graph of ΔK_i Fuzzy regular output surface graph of ΔK_d

Figure 31: Fuzzy regular surfaces of output variables.

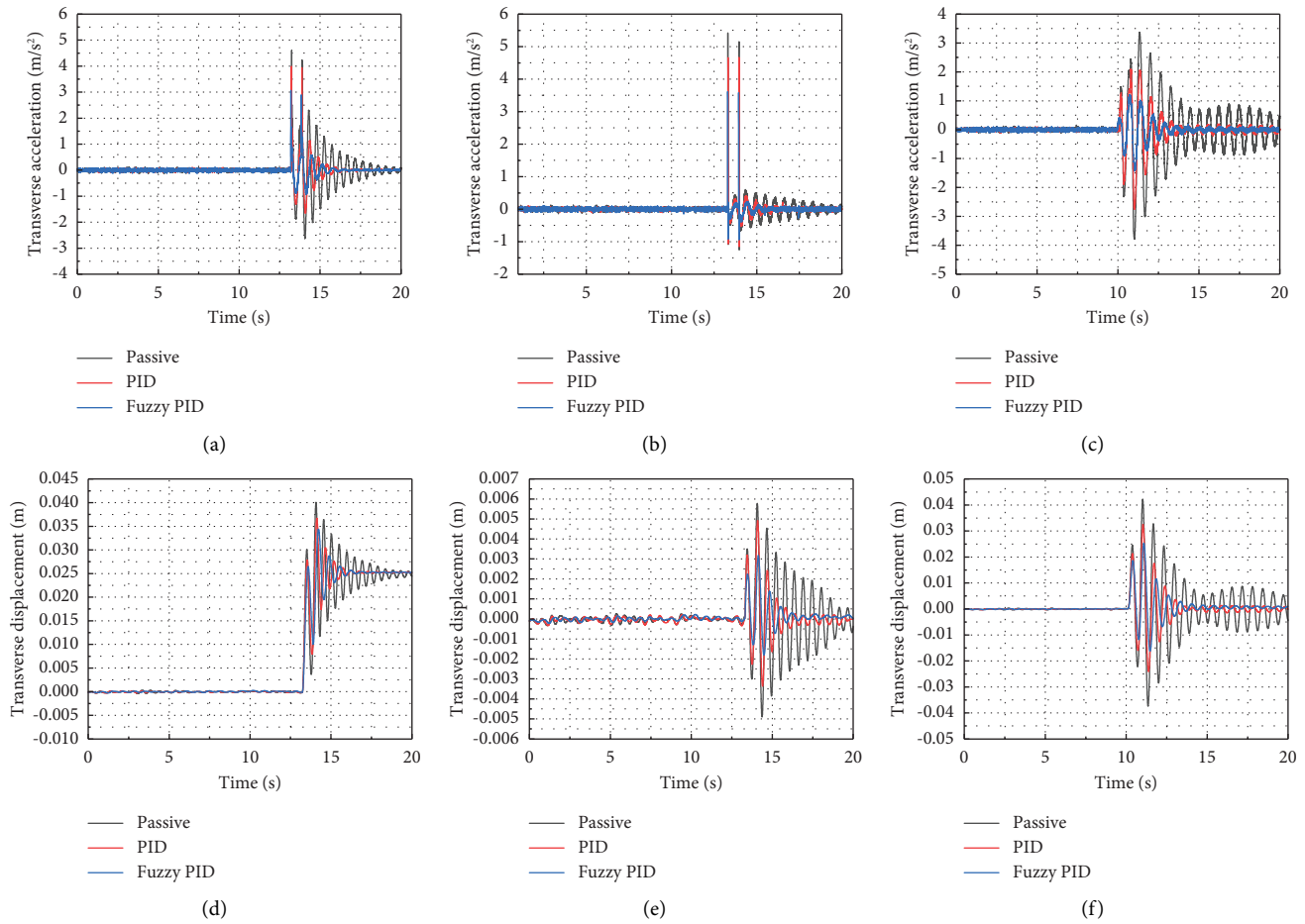

Figure 32: Transverse vibrations comparison of the three cases: (a) and (d) interface misalignment; (b) and (e) local bulge; (c) and (f) bending deformation.

Table 7: Control results of interface misalignment.

	RMS	Max	Reduction percentage of RMS	Reduction percentage of Max
Passive	0.4852	4.6070	—	—
PID	0.2732	3.9851	43.7%	13.5%
Fuzzy PID	0.1875	3.0599	61.4%	33.6%

Table 8: Control results of the local bulge.

	RMS	Max	Reduction percentage of RMS	Reduction percentage of Max
Passive	0.1922	5.4154	—	—
PID	0.1414	4.6653	26.4%	13.9%
Fuzzy PID	0.1054	3.6134	45.2%	33.3%

Table 9: Control results of bending deformation.

	RMS	Max	Reduction percentage of RMS	Reduction percentage of Max
Passive	0.8166	3.3741	—	—
PID	0.4467	2.1044	45.3%	37.6%
Fuzzy PID	0.2926	1.8215	64.2%	46%

As shown in Tables 7–9, under the interface misalignment fault, the root mean square of the acceleration was reduced by 43.7% and 61.4%, respectively, and the maximum value was reduced by 13.5% and 33.6%, respectively. Under the local bulge fault, the root mean square was reduced by 26.4% and 45.2%, respectively, and the maximum value was reduced by 13.9% and 33.3%, respectively. Under the bending deformation fault, the root mean square was reduced by 45.3% and 64.2%, respectively, and the maximum value was reduced by 37.6% and 46%, respectively. The result shows that the stability of container operation is improved when the PID and fuzzy PID controllers are applied to the semiactive vibration reduction control of the MR damper, and the performance controlled by the fuzzy PID controller is better than the PID controller.

5. Conclusions

First, the virtual prototype model for transverse vibration of the hoisting conveyance was established. Subsequently, the vibration response characteristics of the container under various single and coupling excitations were obtained in Adams. The results showed that the gap between two adjacent steel guides has little effect on the responses of the transverse vibrations of the hoisting container, and the interface misalignment and local bulge would contribute to a more serious vibration compared to the situations of guide bending and tilt. Also, several coupling excitations can cause severe vibrations; the amplitudes of the oscillating displacements are so small that they can be ignored while the oscillating accelerations cannot be ignored. Eventually, a new type of roller cage shoe with a magnetorheological damper was put forward to decrease the impact acceleration. Based on the hyperbolic tangent model of magnetorheological dampers, semiactive fuzzy PID methods were studied by the joint simulation of Adams and MATLAB/Simulink to explore the vibration suppression of the container. The results showed that the fuzzy PID method has a certain effect on the reduction of the transverse vibrations of the hoisting container. Further nonlinear control methods should be explored to obtain a better control effect.

Data Availability

The data used to support the findings of this study are available from the corresponding author upon request.

Conflicts of Interest

The authors declare that there are no conflicts of interest regarding the publication of this article.

Acknowledgments

The authors gratefully acknowledge the support of National Natural Science Foundation of China (Grant no. 51805273), the support of Qing Lan Project of Jiangsu Province, and the support of Priority Academic Program Development of Jiangsu Higher Education Institutions (PAPD).

References

[1] J. Yao, Y. Ma, C. Ma, X. Xiao, and T. Xu, "Effect of misalignment failures of steel guides on impact responses in friction mine hoisting systems," *Engineering Failure Analysis*, vol. 118, Article ID 104841, 2020.

[2] Y. Ma, J. Yao, C. Ma, and X. Xiao, "Pattern recognition of rigid hoist guides based on support vector machine," *Advances in Mechanical Engineering*, vol. 10, no. 12, 2018.

[3] J. Yao, X. Deng, C. Ma, and T. Xu, "Investigation of dynamic load in s mine hoisting systems induced by drum winding," *Shock and Vibration*, vol. 2021, Article ID 4756813, 13 pages, 2021.

[4] G. Wang, X. Xiao, and Y. Liu, "Dynamic modeling and analysis of a mine hoisting system with constant length and variable length," *Mathematical Problems in Engineering*, vol. 2019, Article ID 4185362, 12 pages, 2019.

[5] Y. Zhu, T. Xu, and J. Yao, "Investigation of transverse vibration suppression of hoisting catenaries in mine hoists by virtual prototype and uniform design," *International Journal of Modelling, Identification and Control*, vol. 41, no. 3, pp. 165–172, 2022.

[6] Y. Guo, D. Zhang, K. Chen, C. Feng, and S. Ge, "Longitudinal dynamic characteristics of steel wire rope in a friction hoisting system and its coupling effect with friction transmission," *Tribology International*, vol. 119, pp. 731–743, 2018.

[7] Y. Guo, D. Zhang, X. Yang, C. Feng, and S. Ge, "Experimental research on effect of wire rope transverse vibration on friction transmission stability in a friction hoisting system," *Tribology International*, vol. 115, pp. 233–245, 2017.

[8] J. Wang, G. Cao, Z. Zhu, Y. Wang, and W. Peng, "Lateral response of cable-guided hoisting system with time-varying length: t," *Proceedings of the Institution of Mechanical Engineers Part C: Journal of Mechanical Engineering Science*, vol. 229, no. 16, pp. 2908–2920, 2015.

[9] C. Ma, J. Yao, X. Xiao, X. Di, and Y. Jiang, "Vibration analysis of winding hoisting system based on ADAMS/cable Journal of physics: conference series," *Journal of Physics: Conference Series*, vol. 1750, no. 1, Article ID 012033, 2021.

[10] G. Cao, X. Cai, N. Wang, W. Peng, and J. Li, "Dynamic response of parallel hoisting system under drive deviation between ropes with time-varying length," *Shock and Vibration*, vol. 2017, p. 6837697, 2017.

[11] Z. Yang, Q. Zhang, R. Zhang, and L. Zhang, "Transverse vibration response of a super high-speed elevator under air

disturbance," *International Journal of Structural Stability and Dynamics*, vol. 19, no. 09, Article ID 1950103, 2019.

[12] Q. Peng, A. Jiang, H. Yuan, G. Huang, S. He, and S. Li, "Study on theoretical model and test method of vertical vibration of elevator traction system," *Mathematical Problems in Engineering*, vol. 2020, Article ID 8518024, 12 pages, 2020.

[13] R. Zhang, C. Wang, Q. Zhang, and J. Liu, "Response analysis of non-linear compound random vibration of a high-speed elevator," *Journal of Mechanical Science and Technology*, vol. 33, no. 1, pp. 51–63, 2019.

[14] R. Zhang, C. Wang, and Q. Zhang, "Response analysis of the composite random vibration of a high-speed elevator considering the nonlinearity of guide shoe," *Journal of the Brazilian Society of Mechanical Sciences and Engineering*, vol. 40, pp. 1–10, 2018.

[15] D. H. Yang, K. Y. Kim, M. K. Kwak, and S. Lee, "Dynamic modeling and experiments on the coupled vibrations of building and elevator ropes," *Journal of Sound and Vibration*, vol. 390, pp. 164–191, 2017.

[16] H. Zhou, S. Zhang, L. Qiu, Z. Wang, and H. Li, "The multi-component coupling horizontal vibration modeling technology of the high-speed elevator and analysis of its influencing factors," *Proceedings of the Institution of Mechanical Engineers Part C: Journal of Mechanical Engineering Science*, vol. 236, no. 11, pp. 5850–5869, 2022.

[17] Q. Zhang, T. Hou, R.-J. Zhang, and J. Liu, "Time-Varying characteristics of the longitudinal vibration of a high-speed traction elevator lifting system," *International Journal of Acoustics and Vibration*, vol. 25, no. 2, pp. 153–161, 2020.

[18] L. Qiu, C. He, G. Yi et al., "Energy-based vibration modeling and solution of high-speed elevators considering the multi-direction coupling property," *Energies*, vol. 13, no. 18, p. 4821, 2020.

[19] M. Benosman, "Lyapunov-based control of the sway dynamics for elevator ropes," *IEEE Transactions on Control Systems Technology*, vol. 22, no. 5, pp. 1855–1863, 2014.

[20] T. X. Nguyen, N. Miura, and A. Sone, "Analysis and control of vibration of ropes in a high-rise elevator under earthquake excitation," *Earthquake Engineering and Engineering Vibration*, vol. 18, no. 2, pp. 447–460, 2019.

[21] X. T. Nguyen, N. Miura, and A. Sone, "Optimal design of control device to reduce elevator ropes responses against earthquake excitation using Genetic Algorithms," *Journal of Advanced Mechanical Design, Systems, and Manufacturing*, vol. 13, no. 2, Article ID JAMDSM0038, 2019.

[22] D. R. Santo, J. M. Balthazar, A. M. Tusset, V. Piccirilo, R. Brasil, and M. Silveira, "On nonlinear horizontal dynamics and vibrations control for high-speed elevators," *Journal of Vibration and Control*, vol. 24, no. 5, pp. 825–838, 2018.

[23] M. Raúl, J. M. Rodríguez-Fortún, A. Gómez, J. A. Roig, and P. González, "Design of semi-active roller guides for high speed elevators Applied mechanics and materials," *Trans Tech Publications Ltd*, vol. 706, pp. 108–116, 2015.

[24] H. Zhang, R. Zhang, Q. He, and L. Liu, "Variable universe fuzzy control of high-speed elevator horizontal vibration based on firefly algorithm and b fuzzy neural network," *IEEE Access*, vol. 9, pp. 57020–57032, 2021.

[25] G. Hu, Q. Liu, R. Ding, and G. Li, "Vibration control of semi-active suspension system with magnetorheological damper based on hyperbolic tangent model," *Advances in Mechanical Engineering*, vol. 9, no. 5, p. 1687814017694581, 2017.

[26] W. Zeng, Q. Jiang, J. Xie, and T. Yu, "A fuzzy-PID composite controller for core power control of liquid molten salt reactor," *Annals of Nuclear Energy*, vol. 139, Article ID 107234, 2020.

[27] Y. Wu, C. Zhang, and Y. Liu, "Design and simulation of fuzzy-PID vector control system based on mine hoist," *Applied Mechanics and Materials*, vol. 300-301, pp. 1486–1489, 2013.

[28] C. Ma, S. Tian, X. Xiao, and Y. Jiang, "Fuzzy Neural Network PID–based constant deceleration compensation device for the brakes of mining hoists," *Advances in Mechanical Engineering*, vol. 12, no. 7, Article ID 168781402093756, 2020.

[29] X. Xiao, J. Wu, Q. Wang, and C. Hu, "Dynamic Analysis and Simulation on Multiplexed Controllable Antiskid Device of Friction Hoist," in *Proceedings of the IEEE International Conference on Information and Automation*, New York, NY, USA, January 2010.

[30] G. Wang, Y. Zhou, and Yapeng Di, "Research on Constant Deceleration Braking Performance of the Disc Braking System for Ultra Deep Mine Hoist," in *Proceedings of the International Conference on Measuring Technology and Mechatronics Automation*, Changsha, China, February 2018.

[31] Q. Wang, D. Liang, and J. Du, "Design of Mining Flameproof Voltage Stabilizing Transformer Adopting Adaptive Fuzzy PID Controller," in *Proceedings of the International Conference on Electrical Machines and Systems*, Hangzhou, China, October 2014.

[32] L. P. Chen, "Mechanical System Dynamics Analysis and Adams Application Course," Tsinghua University Press, Beijing, China, 2005.